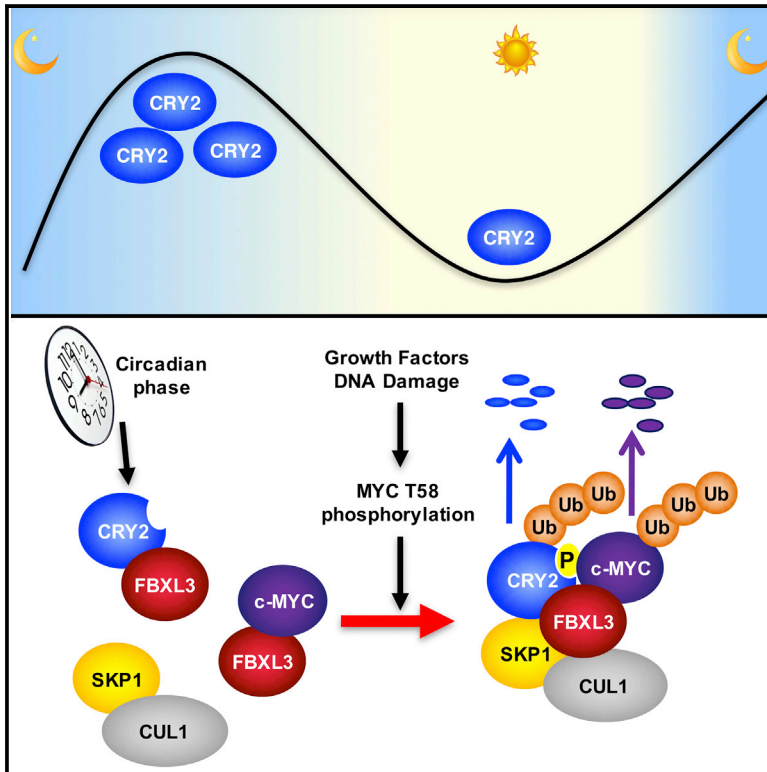


CRY2 and FBXL3 Cooperatively Degrade c-MYC

Graphical Abstract



Authors

Anne-Laure Huber, Stephanie J. Papp, Alanna B. Chan, ..., Zhizhong Li, Christian M. Metallo, Katja A. Lamia

Correspondence

klamia@scripps.edu

In Brief

Circadian disruption increases the risk of many types of cancer. Huber et al. demonstrate that the circadian clock protein CRY2 recruits T58-phosphorylated c-MYC to SCF^{FBXL3}, thus promoting its ubiquitination and degradation. This unexpected function of CRY2 may contribute to circadian protection from tumorigenesis.

Highlights

- Loss of CRY2 stabilizes c-MYC and enhances cellular transformation
- CRY2 can function as a co-factor for the SCF substrate adaptor FBXL3
- c-MYC phosphorylated on threonine 58 (T58) interacts with CRY2
- SCF^{FBXL3+CRY2} promotes the ubiquitylation and turnover of c-MYC

Accession Numbers

GSE89018

Che sistema hanno usato per la trasfezione?

Che sistema hanno usato per la mutagenesi?



CRY2 and FBXL3 Cooperatively Degrade c-MYC

Anne-Laure Huber,¹ Stephanie J. Papp,¹ Alanna B. Chan,¹ Emma Henriksson,^{1,4} Sabine D. Jordan,¹ Anna Kriebs,¹ Madelena Nguyen,¹ Martina Wallace,² Zhizhong Li,³ Christian M. Metallo,² and Katja A. Lamia^{1,5,*}

¹Department of Chemical Physiology, The Scripps Research Institute, 10550 North Torrey Pines Road, MB31, La Jolla, CA 92037, USA

²Department of Bioengineering, University of California, San Diego, La Jolla, CA 92093, USA

³Drug Discovery Oncology Unit, Genomics Institute of the Novartis Research Foundation and Novartis Institutes for Biomedical Research, 10675 John J. Hopkins Drive, San Diego, CA 92121, USA

⁴Department of Clinical Sciences, CRC, Lund University, Malmö 20502, Sweden

⁵Lead Contact

*Correspondence: klamia@scripps.edu

<http://dx.doi.org/10.1016/j.molcel.2016.10.012>

SUMMARY

For many years, a connection between circadian clocks and cancer has been postulated. Here we describe an unexpected function for the circadian repressor CRY2 as a component of an FBXL3-containing E3 ligase that recruits T58-phosphorylated c-MYC for ubiquitylation. c-MYC is a critical regulator of cell proliferation; T58 is central in a phosphodegron long recognized as a hotspot for mutation in cancer. This site is also targeted by FBXW7, although the full machinery responsible for its turnover has remained obscure. CRY1 cannot substitute for CRY2 in promoting c-MYC degradation. Their unique functions may explain prior conflicting reports that have fueled uncertainty about the relationship between clocks and cancer. We demonstrate that c-MYC is a target of CRY2-dependent protein turnover, suggesting a molecular mechanism for circadian control of cell growth and a new paradigm for circadian protein degradation.

INTRODUCTION

Mice harboring genetically disrupted clock function (Fu et al., 2002; Geyfman et al., 2012; Janich et al., 2011; Lee et al., 2010; Ozturk et al., 2009) or subjected to experimental jet lag (Papagianakopoulos et al., 2016; Van Dycke et al., 2015) exhibit altered rates of tumor formation. Analysis of epidemiological studies spurred the World Health Organization to designate circadian disruption as a probable carcinogen (Straif et al., 2007). Although several molecular connections have been suggested (Gaddameedhi et al., 2011; Gotoh et al., 2014, 2015; Papp et al., 2015; Unsal-Kaçmaz et al., 2005, 2007), the relationship between clocks and cancer is not well understood and remains controversial (West and Bechtold, 2015). Mammalian clocks involve a transcriptional feedback loop (Partch et al., 2014): CLOCK and BMAL1 drive expression of period (PER1–3) and cryptochrome (CRY1,2) repressors, which inhibit CLOCK:BMAL1, resulting in oscillating transcription of thousands of genes (Panda et al.,

2002; Storch et al., 2002). Ubiquitylation of CRY1/2 by Skp1, Cul1, F-box protein ubiquitin ligase complex (SCF^{FBXL3}) is important for setting clock speed (Busino et al., 2007; Godinho et al., 2007; Siepka et al., 2007).

c-MYC plays a critical role in cell proliferation, and its levels are tightly controlled by regulated protein degradation (Farrell and Sears, 2014). When c-MYC is phosphorylated on T58, it is targeted by SCF^{FBXW7} for ubiquitylation and proteasomal degradation (Popov et al., 2007; Welcker et al., 2004; Yada et al., 2004). However, FBXW7 preferentially interacts with doubly phosphorylated substrates (Hao et al., 2007; Welcker and Clurman, 2008), and, in some contexts, mutation of T58 to a non-phosphorylatable residue stabilizes c-MYC more than ablation of SCF^{FBXW7} does (Chakraborty and Tansey, 2009; Popov et al., 2007; Salghetti et al., 1999). It has therefore been suggested that one or more additional E3 ligase(s) also stimulate(s) the proteolysis of c-MYC phosphorylated on T58 (Thomas and Tansey, 2011). Understanding the mechanisms leading to destruction of T58-phosphorylated c-MYC is important because the sequence surrounding c-MYC T58 has long been recognized as a hotspot of mutations in human cancer (Bhatia et al., 1993, 1994). Moreover, disrupted turnover of singly T58-phosphorylated MYC is associated with MYC stabilization and tumorigenesis (Malempati et al., 2006). Here we demonstrate that CRY2 and SCF^{FBXL3} drive proteolytic turnover of T58-phosphorylated c-MYC via binding of phospho-T58 to CRY2 near its binding interface with FBXL3. These findings suggest that CRY2-driven cycles of c-MYC turnover represent a previously unappreciated mode of clock output that affects cancer susceptibility because of circadian disruption.

RESULTS

Loss of *Cry2* Enhances Proliferation and Transformation

To examine the roles of CRY1 and CRY2 in growth control, we performed proliferation and transformation assays using five independently isolated sets of primary mouse fibroblasts derived from wild-type, *Cry1*^{-/-}, and *Cry2*^{-/-} littermates. We infected three independently derived primary mouse embryonic fibroblast (MEF) cell lines and two fibroblast cell lines derived from adult skin biopsies of each genotype with viruses expressing the oncogenes *c-MYC* or *HRAS*^{V12} or small hairpin RNA (shRNA) targeting the tumor suppressor *P53*. To avoid selection of clonal

Main
Question

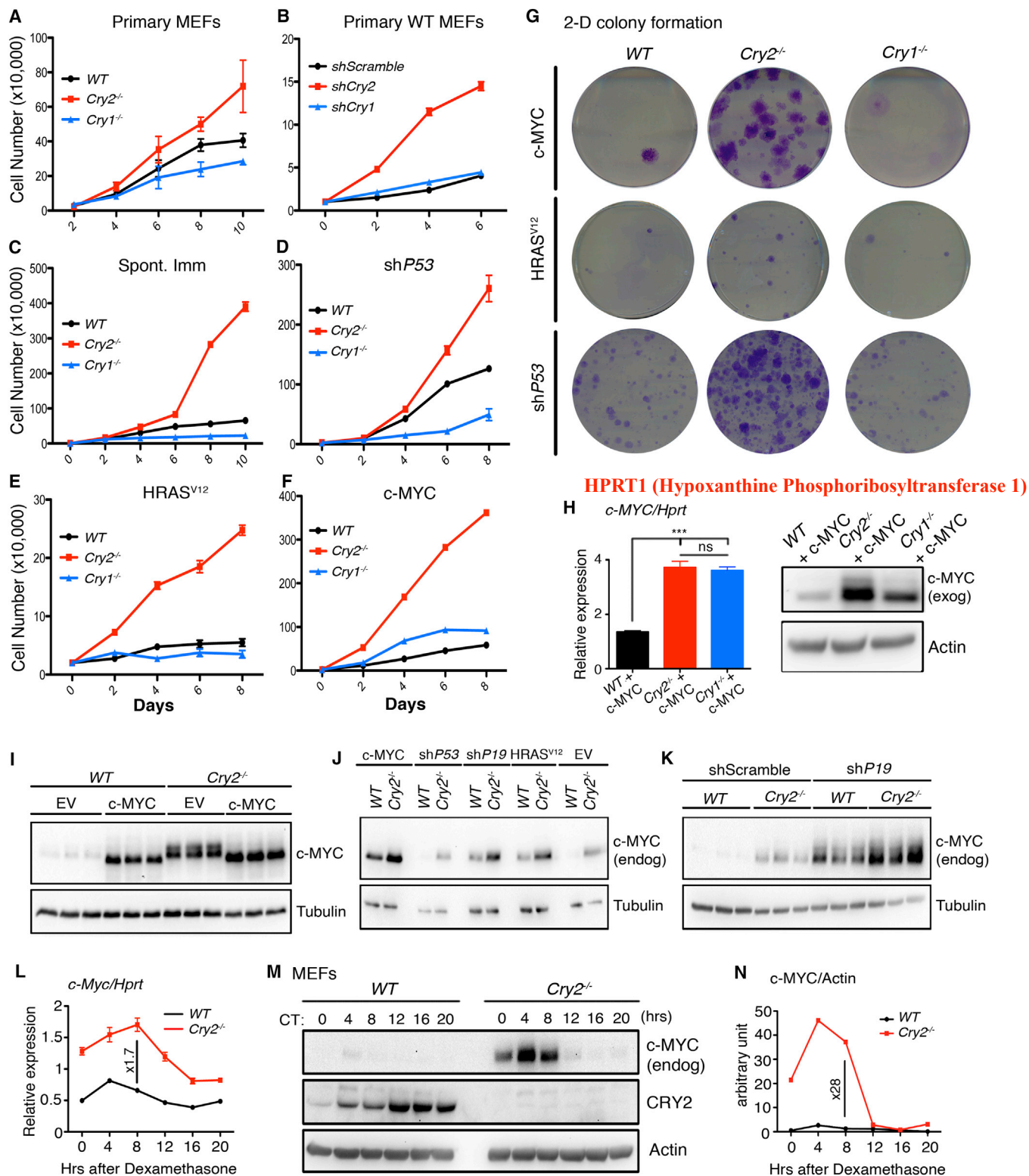


Figure 1. CRY2 Deletion Enhances Cell Growth and Transformation

(A–G) Proliferation (A–F) and colony formation in two-dimensional culture (G) in primary MEFs of the indicated genotypes subjected to the 3-day transfer, inoculum 3×10^5 cells (3T3) protocol (Spont. Imm.) or stably expressing the indicated plasmids. Data represent the **mean \pm SD for triplicate samples (A–F) or a typical result**

(legend continued on next page)

lines that may not accurately reflect the effects of *Cry1/2* deletion, we characterized heterogeneous pools of virally transduced cells subjected to antibiotic selection for less than 2 weeks. In all contexts, *Cry2* deficiency enhanced proliferation and colony formation (Figures 1A–1G), indicating surprisingly widespread cooperative effects with multiple oncogenic changes. Similarly, wild-type fibroblasts stably expressing shRNA targeting *Cry2* were more highly proliferative than those expressing control sequences or shRNA targeting *Cry1* (Figure 1B). Mostly, loss of *Cry1* had little or no effect on proliferation or transformation; however, in the context of *P53* depletion, cells lacking *Cry1* were less sensitive to transformation (Figures 1D and 1G). This is consistent with the increased survival of *Cry1/2*-deficient mice in a *P53*^{-/-} background (Ozturk et al., 2009) and suggests that CRY1- and CRY2-specific functions may explain the different effects on tumor formation in previous studies of tumorigenesis in *Cry1*^{-/-};*Cry2*^{-/-} mice (Fu and Kettner, 2013; Lee et al., 2010). Loss of *Cry2* was not sufficient to transform primary cells, and *Cry2*^{-/-} cells did not robustly form colonies in soft agar with a single oncogenic insult (*P53* depletion or expression of either *HRAS*^{V12} or *c-MYC*; data not shown), indicating that CRY2 is not a tumor suppressor per se.

Loss of *Cry2* Stabilizes c-MYC

Enhanced proliferation and colony formation of *Cry2*^{-/-} cells expressing either *c-MYC* or shRNA targeting *P53* suggests that the loss of CRY2 affects multiple pathways that control cell growth. For example, cooperation with *c-MYC* indicates a defect in *P53* function, whereas cooperation with *P53* depletion could be explained by enhanced MYC activity. In assessing the efficiency of viral oncogene expression, we found that, although overexpressed human *c-MYC* mRNA is somewhat (~2.2-fold) elevated in both *Cry1*^{-/-} and *Cry2*^{-/-} cells compared with wild-type controls, c-MYC protein abundance is highly increased specifically in *Cry2*^{-/-} cells (Figure 1H), suggesting that the loss of *Cry2* alters c-MYC post-transcriptional regulation. Upon further examination, we found that overexpression of human c-MYC repressed the endogenous *c-Myc* transcript in wild-type and *Cry2*^{-/-} fibroblasts as expected (Figure S1A, available online). Strikingly, overexpressed human c-MYC and especially endogenous mouse c-MYC protein levels are elevated in *Cry2*^{-/-} cells compared with controls (Figure 1I). Because elevated c-MYC protein could contribute to the enhanced colony formation observed in *Cry2*^{-/-} cells upon depletion of *P53* or overexpression of mutant RAS, we measured endogenous c-MYC protein in those cells as well as in cells expressing shRNA targeting *P19Arf* (an upstream regulator of *P53*). In every case, c-MYC is increased in *Cry2*^{-/-} cells compared with controls (Figures 1J and 1K). High levels of c-MYC induce apoptosis via *P53*, so

defective *P53* signaling can enable MYC protein accumulation. Increased c-MYC in *Cry2*^{-/-} cells expressing shRNA targeting *P53* or *P19Arf* cannot be attributed to such a defect. Taken together, these data indicate that CRY2 regulates c-MYC protein levels.

In primary MEFs, following the induction of synchronized circadian rhythms by dexamethasone (Balsalobre et al., 2000), endogenous *c-Myc* mRNA is rhythmically expressed, consistent with an earlier report (Fu et al., 2002), and its peak is ~1.7-fold higher in *Cry2*^{-/-} cells (Figure 1L). Strikingly, c-MYC protein exhibits a high-amplitude circadian rhythm, and peak c-MYC protein is much higher in *Cry2*^{-/-} compared with wild-type cells (Figures 1M, 1N, and S1B). Thus, c-MYC protein levels are elevated in *Cry2*-deficient cells regardless of the endogenous or viral promoter elements controlling its transcription, strongly suggesting that CRY2 modulates post-transcriptional regulation of c-MYC. Metabolic tracer analysis of primary MEFs revealed changes consistent with enhanced MYC and increased proliferative and transformative capacity in *Cry2*^{-/-} primary MEFs (Figures S1C–S1G). Elevated levels of endogenous c-MYC protein in *Cry2*^{-/-} cells could explain the observed cooperativity between CRY2 loss and *HRAS*^{V12} expression or *P53* depletion; other changes in *Cry2*^{-/-} cells probably contribute to the increase in transformation by c-MYC in *Cry2*^{-/-} cells compared with wild-type controls. Here we focus on understanding how CRY2 regulates c-MYC protein levels.

Post-transcriptionally enhanced c-MYC protein levels could reflect increased production and/or decreased decay. The incorporation of ³⁵S-methionine into c-MYC was slightly elevated in *Cry2*^{-/-} cells compared with controls, similar to the ~2-fold change in *c-Myc* mRNA, suggesting that translation of *c-Myc* is not specifically increased in the absence of CRY2 (Figure S2A). To determine whether the c-MYC protein half-life is increased in *Cry2*^{-/-} cells, we examined c-MYC protein turnover after addition of the translation inhibitor cycloheximide (CHX) in wild-type and *Cry2*^{-/-} embryonic and adult fibroblasts (Figures 2A–2C, S2B, and S2C). Consistent with previous studies, c-MYC has a very short half-life in wild-type cells, as evidenced by the rapid turnover within 15–20 min. In *Cry2*^{-/-} cells, c-MYC is stabilized in the presence of CHX. Notably, re-introducing CRY2 in these cells decreased the half-life of endogenous c-MYC (Figures 2B, 2C, S2B, and S2C). Thus, CRY2 regulates the half-life of endogenous c-MYC.

Because CRY2 can repress transcription and targets many unique sites in chromatin independent of other circadian factors (Koike et al., 2012), we hypothesized that it could alter c-MYC stability via transcription of one or more effectors. However, qPCR showed no alterations of transcripts encoding regulators of c-MYC degradation that would explain the observed

(G) from a representative experiment of at least three experiments of each type performed in three sets of MEFs derived from littermate animals. Similar results were obtained using two sets of adult skin fibroblasts derived from littermate animals.

(H) mRNA (left) and protein (right) measured by immunoblot (IB) or qPCR from MEFs of the indicated genotypes stably overexpressing c-MYC.

(I–K) Proteins measured by IB from adult skin fibroblasts (I and J) or MEFs (K) of the indicated genotypes stably expressing the indicated plasmids.

(L and M) Endogenous mRNA (L) and proteins (M) detected by qPCR or IB in MEFs of the indicated genotypes and harvested at the indicated times. CT, hours after circadian synchronization.

(N) Quantitation of the IB data shown in (M).

See also Figure S1.

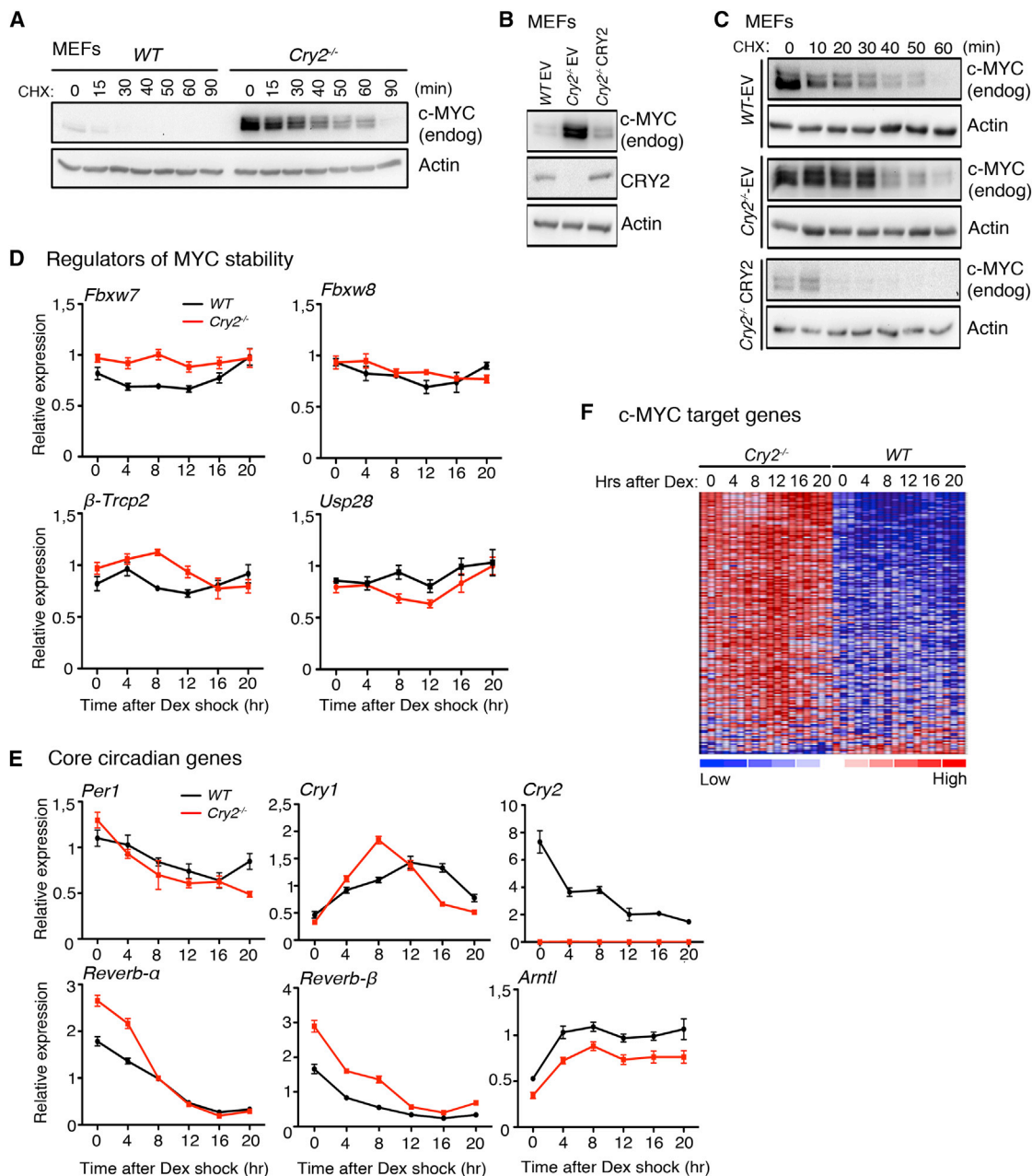


Figure 2. CRY2 Deletion Increases c-MYC Stability

(A–C) Endogenous proteins detected by IB in MEFs of the indicated genotypes expressing the indicated plasmids and harvested at the indicated times. CHX, minutes after cycloheximide.

(B) Samples from time 0 for all cell lines shown in (A) loaded together.

(D and E) Transcripts measured by qPCR in primary MEFs of the indicated genotypes at the indicated times after synchronization of circadian rhythms with dexamethasone treatment. Data represent the mean \pm SD for three biological replicates, each measured in triplicate.

(F) Heatmap from RNA sequencing in primary MEFs at the indicated times after circadian synchronization. Colors represent high (red) to low (blue) expression. Gene names and expression values are provided in Table S2.

See also Figure S2 and Tables S1 and S2.

stabilization of c-MYC (Figure 2D). Deep sequencing of RNA isolated from wild-type and *Cry2*^{-/-} primary MEFs over a full circadian cycle revealed 865 transcripts that were altered by the loss of CRY2 (false discovery rate [FDR] < 0.01; Table S1) but no

obvious explanation for c-MYC stabilization. Notably, core circadian transcripts oscillate in *Cry2*^{-/-} cells (Figure 2E) because CRY1 can support circadian rhythms in the absence of CRY2 (Ukai-Tadenuma et al., 2011). Although prolonged elevation of

c-MYC can lead to general amplification of transcription (Lin et al., 2012; Nie et al., 2012), transcripts that are likely to be directly regulated by c-MYC (Sabò et al., 2014; Walz et al., 2014) are overrepresented among those that are significantly altered by deletion of *Cry2* (~14% of MYC targets identified in Sabò et al., 2014, versus ~4% of the genome are altered by *Cry2* deletion; Figures S2D and S2E). Furthermore, gene set enrichment analysis (GSEA) (Subramanian et al., 2007) detected significantly enriched expression of a hallmark set of c-MYC target genes (Liberzon et al., 2015) in *Cry2*^{-/-} cells (Figures 2F and S2F; Table S2), suggesting that the highly elevated c-MYC protein observed in *Cry2*^{-/-} cells is transcriptionally active.

CRY2 and FBXL3 Cooperatively Bind c-MYC

Because transcriptional changes did not appear to explain the greatly increased c-MYC stability in *Cry2*^{-/-} cells, we investigated other ways in which CRY2 could affect c-MYC. Expression of CRY2 did not prevent interaction of c-MYC with MAX, FBXW7, or βTRCP (Figures S3A–S3C). Surprisingly, overexpressed c-MYC co-purifies with overexpressed CRY2 (Figure 3A), and this interaction requires the N-terminal regulatory domain of c-MYC (Figures 3B and 3C). Because CRY2 associates with the SCF E3 ligase substrate receptor FBXL3, we considered the possibility that SCF^{FBXL3} acts on c-MYC. Although previous studies have not identified c-MYC in FBXL3-containing protein complexes (Busino et al., 2007), mass spectrometry often produces false negative results, especially for F box proteins, which stimulate the degradation of their substrate partners (Yumimoto et al., 2012). Proteins of very low abundance like c-MYC are most likely to be missed. Indeed, we found that FBXL3 can interact with c-MYC (Figure 3D) and that CRY2 enhances the FBXL3-MYC interaction (Figure 3E). We also observed interactions between CRY2, FBXL3, and c-MYC when all three were produced by in vitro transcription and translation (Figure S3D), suggesting that they interact directly.

Aligning SKP1 in the crystal structures of SKP1-CRY2-FBXL3 (Xing et al., 2013), SKP1-SKP2-CUL1-RBX1 (Zheng et al., 2002), SKP1-FBXW7-CYCLIN E (Hao et al., 2007), and SKP1-SKP2-CKS1-p27KIP1 (Hao et al., 2005) reveals that the orientation of CRY2 relative to FBXL3 overlaps with that of the adaptor CKS1 relative to SKP2/FBXL1 and leaves a large open space between CRY2, FBXL3, and the RBX1 active site, including the position occupied by the CYCLIN E and p27KIP1 degron peptides (Figures 3F and S3E). These findings led us to hypothesize that, in addition to being a substrate for SCF^{FBXL3}, CRY2 could act as a co-factor to recruit additional substrates, including c-MYC, to SCF^{FBXL3}. Thus, the observed stabilization of c-MYC in the absence of CRY2 may reflect a loss of SCF^{FBXL3}-mediated ubiquitylation of c-MYC. Importantly, c-MYC protein was greatly increased in fibroblasts expressing either of two shRNAs targeting *Fbxl3* (Figures 3G and S3F), similar to what we observed in *Cry2*-deficient cells and consistent with a role for a CRY2-FBXL3 heterodimer in ubiquitylation of c-MYC.

Our model leads to the prediction that mutations in CRY2 or FBXL3 that reduce their interaction with each other would reduce their interaction with c-MYC. Several point mutations in CRY2 that disrupt its association with FBXL3 without altering interactions

with CLOCK, BMAL1, or PER2 have been described (Xing et al., 2013). The interaction of those mutants with c-MYC is abolished (Figure 3H). In addition, mutation of the FBXL3 C-terminal tryptophan, which decreases its interaction with CRY2 (Xing et al., 2013), also reduces the interactions of CRY2 and FBXL3 with c-MYC (Figure 3I). To further examine the ability of CRY2, FBXL3, and c-MYC to form a trimeric complex, we serially immunoprecipitated overexpressed CRY2 and FBXL3 and observed progressive enrichment of c-MYC (Figures 3J and S3G).

CRY2-FBXL3 Promotes c-MYC Ubiquitylation

We measured the ubiquitylation of overexpressed c-MYC in the presence or absence of overexpressed CRY2 and FBXL3 and found that CRY2 and FBXL3 together stimulate c-MYC ubiquitylation (Figures 4A, S4A, and S4B). Deletion of the F box (ΔF) in FBXL3 prevents its association with SKP1 and CUL1 and thus prevents formation of the active SCF^{FBXL3} complex. Consistent with the observed loss of CUL1 binding, although FBXL3ΔF interacts with CRY2 and c-MYC, it did not promote c-MYC ubiquitylation. Mutation of the FBXL3 C-terminal tryptophan, which inhibits FBXL3-CRY2 interaction, reduced the recruitment of c-MYC to FBXL3 and blocked its ubiquitylation (Figures S4A and S4B). As reported by others (Yumimoto et al., 2013), we found that CRY2 promotes the association of FBXL3 with CUL1 (Figures S4B and S4C), further supporting the importance of CRY2 as a scaffold for formation of a fully active SCF^{FBXL3} complex to promote ubiquitylation and turnover of c-MYC.

We examined the contributions of CRY2 and FBXL3 to c-MYC protein turnover in cells overexpressing c-MYC and either FBXW7 or FBXL3 and CRY2. The steady-state level of overexpressed c-MYC was decreased by overexpression of CRY2 and FBXL3 to a similar extent as overexpression of the established c-MYC SCF substrate adaptor FBXW7 (Figures 4B and S4D). The half-life of overexpressed c-MYC is much longer than that of the endogenous protein, likely because of saturation of endogenous systems involved in c-MYC degradation. Using either cycloheximide treatment or ³⁵S-methionine labeling to measure c-MYC protein turnover, we observed a similar increase in c-MYC turnover with expression of either FBXW7 or FBXL3 and CRY2 (Figures 4C–4F). The effects of FBXL3 and CRY2 on MYC half-life are reduced by mutations (FBXL3W428A or CRY2F428D) that disrupt the CRY2-FBXL3 interaction (Figures 4G and 4H), further supporting our hypothesis that the CRY2-FBXL3 heterodimer promotes c-MYC ubiquitylation.

To examine the effects of CRY2 and SCF^{FBXL3} on the half-life of endogenous c-MYC, we used shRNA knockdown of *Fbxl3* and *Fbxw7* in primary embryonic and adult fibroblasts. Decreasing FBXW7 stabilizes c-MYC in both wild-type and *Cry2*^{-/-} cells, whereas depleting FBXL3 stabilizes c-MYC in wild-type but not in *Cry2*^{-/-} cells (Figures 4I–4L, S4E, and S4F), demonstrating that CRY2 is required for FBXL3- but not FBXW7-dependent effects on c-MYC stability. Finally, we examined the effect of *Fbxl3* disruption in the context of complete genetic deletion of *Fbxw7* using Cre-mediated recombination in primary fibroblasts. Depletion of *Fbxl3* increased c-MYC protein stability regardless of the presence or absence of *Fbxw7*

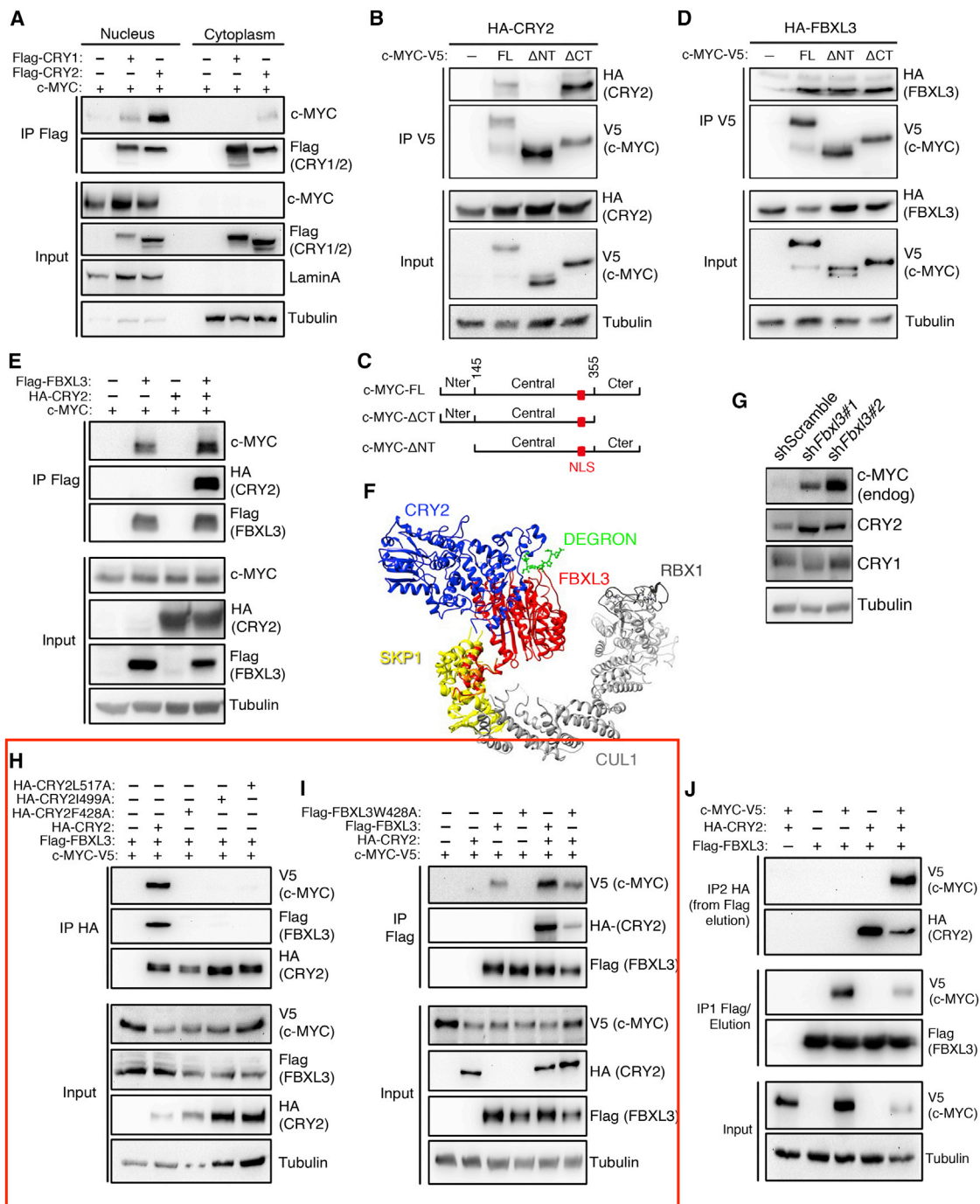


Figure 3. c-MYC Forms a Trimeric Complex with CRY2 and FBXL3

(A, B, D, E, and H–J) Proteins detected by IB following FLAG, HA, or V5 IP from nuclear and cytoplasmic fractions or whole-cell lysates from 293T cells expressing the indicated plasmids.

(C) Schematic of the wild-type and amino- or carboxy-terminal deletion mutants of c-MYC used in the experiments shown in (B) and (D).

(F) Superposition of crystal structures from Protein Data Bank accession numbers 1LDK (SKP1-SKP2-CUL1-RBX1), 2OVR (SKP1-FBW7-CYCEDEGN), 2AST (SKP1-SKP2-CKS1-p27KIP1), and 4I6J (SKP1-FBXL3-CRY2).

(G) Proteins detected by IB in whole-cell lysates of wild-type MEFs expressing the indicated viral shRNA.

See also Figure S3.

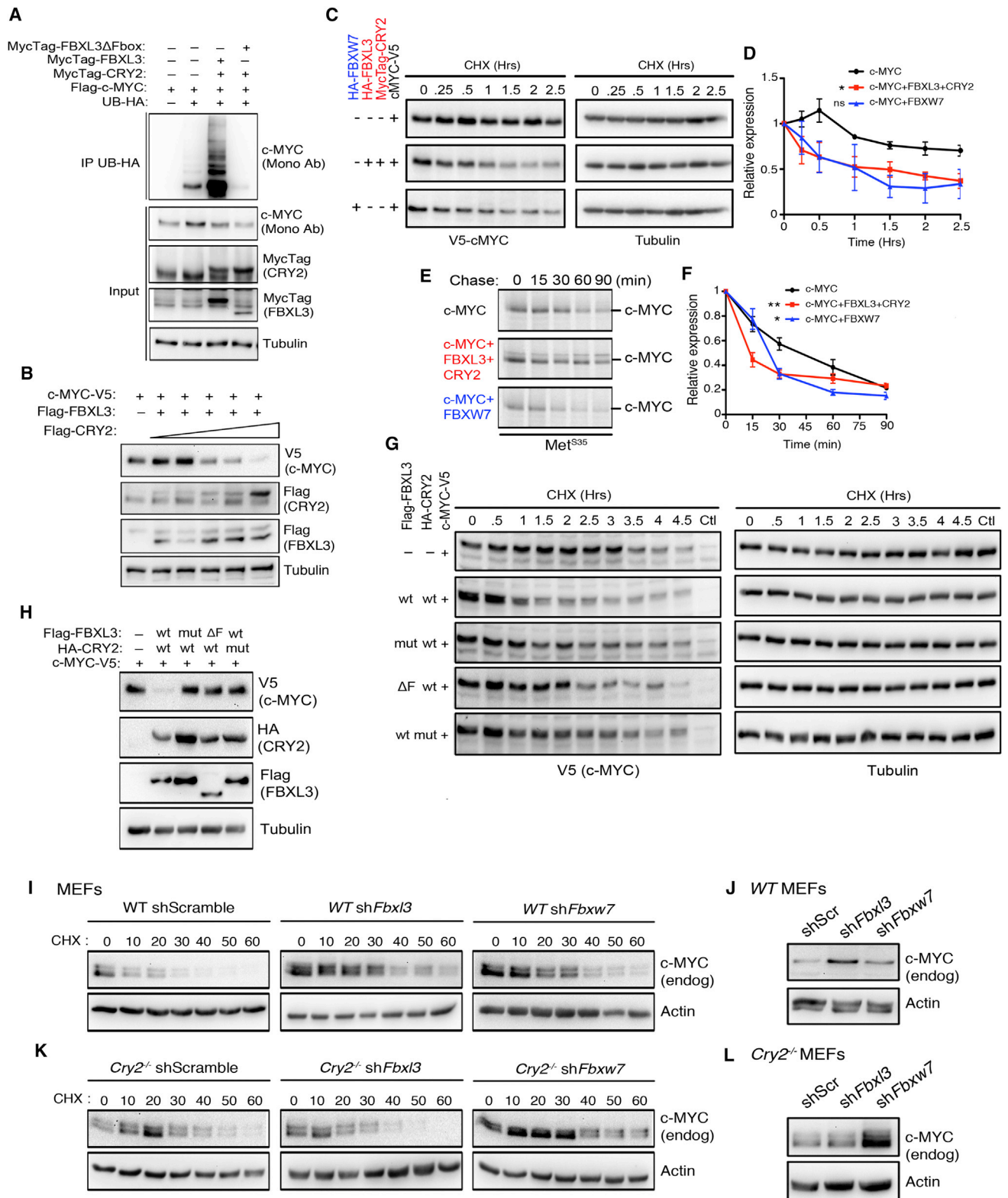


Figure 4. CRY2 Is an Essential Component of SCF^{FBXL3}-Driven c-MYC Ubiquitylation

(A–C, G, H, I–L) Proteins detected by IB following HA IP (A) or in whole-cell lysates (B, C, G, and H) from 293T cells expressing the indicated plasmids or from primary MEFs of the indicated genotypes expressing the indicated plasmids (I–L) and following treatment with CHX for the indicated times (C, G, I, and K).

(legend continued on next page)

(Figures S4G–S4I), demonstrating that these two F-box SCF substrate adaptors represent independent pathways for destabilizing c-MYC.

CRY2-FBXL3 Binds c-MYC Phospho-T58

Phosphorylation of T58 is a primary determinant of c-MYC stability (Gregory et al., 2003; Malempati et al., 2006; Salghetti et al., 1999; Yada et al., 2004). A recent structure of CRY2 bound to a small molecule revealed a conserved, ordered phosphate-binding loop (P loop) on the surface of CRY2 (Nangle et al., 2013) that has also been observed in a conserved region of photolyases (Hitomi et al., 2009), although no phosphorylated partners have been identified. Aligning this structure with our model, we found that this P loop would be located near the CRY2-FBXL3 interface (Figure 5A), suggesting that c-MYC interaction with CRY2-FBXL3 could be regulated by phosphorylation. Because phosphorylation of T58 is a well-established driver of c-MYC proteolysis and because phosphorylation of T58 occurs only after phosphorylation of S62, we examined whether either modification alters the interaction of c-MYC with CRY2-FBXL3. Mutation of T58 and/or S62 to a non-phosphorylatable amino acid greatly reduced the interaction between CRY2 and c-MYC (Figures 5B and S5A) but had little effect on the interaction between c-MYC and FBXL3 when CRY2 was not overexpressed (Figure 5C).

To investigate whether phosphorylated T58 interacts directly with CRY2-FBXL3, we used biotinylated synthetic peptides derived from the sequence of c-MYC surrounding either phosphorylated (P) or non-phosphorylated (NP) threonine at the position corresponding to T58 or a doubly phosphorylated peptide (DP) corresponding to c-MYC phosphorylated on both T58 and S62. Although FBXL3 interacts weakly with all three peptides (Figure 5D, middle immunoprecipitations [IPs]), CRY2 interacts preferentially with the peptide containing phospho-T58 (Figure 5D, left IPs). When purified CRY2 and FBXL3 are combined, the resulting heterodimer exhibits strongly phospho-specific binding to the c-MYC-derived peptide phosphorylated only on the residue corresponding to T58 (Figure 5D, right IPs). **Mutation of the reported CRY2 P loop decreases binding to the T58-phosphorylated c-MYC peptide in vitro and to overexpressed c-MYC in cells (Figures 5E and S5B–S5D), suggesting that this phospho-specific interaction involves direct binding between phosphorylated T58 and the P loop on the surface of CRY2.**

We also examined the role of the CRY2 P loop and c-MYC T58 phosphorylation in CRY2- and FBXL3-driven effects on c-MYC protein turnover. Although overexpression of CRY2 and FBXL3 or of FBXL7 decreases the stability of wild-type c-MYC (Figures 4C–4F), the same manipulations do not significantly increase turnover of c-MYCT58A (Figures 5F–5I and S5E). Mutation of the CRY2 P loop also decreases the effect of CRY2 and FBXL3 on c-MYC turnover (Figure 5J), supporting the idea

that phosphorylation of T58 enhances the interaction of c-MYC with CRY2 and FBXL3 by binding the CRY2 P loop. Lending further support to the model that CRY2 and FBXL3 drive degradation of T58-phosphorylated c-MYC, c-MYCT58A is much less efficiently ubiquitinated than wild-type c-MYC when FBXL3 and CRY2 are overexpressed (Figure S5F).

A Role for CRY2-FBXL3-MYC in Tumors

To investigate whether this model may have relevance for human cancer, in which c-MYC is a well-established major driver, we examined the relationship between CRY2 and c-MYC in human tumor-derived cells. By ranking 1,059 cell lines in the Cancer Cell Line Encyclopedia (CCLE) by CRY2 mRNA expression (Table S3), we selected several among those with the lowest CRY2 for further examination. Exogenous expression of wild-type CRY2 reduced c-MYC protein, proliferation, and anchorage-independent growth in SW480 colon cancer and A549 lung cancer cells (Figures 6A–6D), suggesting that CRY2 may be rate-limiting for c-MYC degradation in tumors harboring low CRY2 expression. Importantly, a CRY2 mutant incapable of binding FBXL3 did not significantly reduce c-MYC protein in these cells (Figures 6A and 6B). Furthermore, we observed a striking and significant correlation of reduced CRY2 expression in tumor samples compared with normal controls for a wide variety of human tissue types (Figure 6E), whereas no such consistent pattern of altered expression was observed for CRY1 (Figure 6F). In bone and lung tumors, FBXL3 is lower than in controls (Figure 6G).

To experimentally test the potential for CRY2 to alter c-MYC in vivo, we bred *Cry2*^{-/-} mice with mice expressing elevated c-MYC in lymphoid cells (Adams et al., 1985) that develop lymphomas after 8 weeks of age. Pre-tumor spleen samples taken from 6-week-old *EμMyc*^{Tg/+};*Cry2*^{-/-} mice contain higher levels of c-MYC protein than those from *EμMyc*^{Tg/+};*Cry2*^{+/+} littermates (Figures 7A and 7B), whereas *c-Myc* mRNA is unchanged (Figure 7C), supporting the hypothesis that deletion of CRY2 enhances c-MYC via a post-transcriptional mechanism in vivo. At the same 6-week-old pre-tumoral stage, we detected small numbers of lymphocytes in Giemsa-stained blood smears from *EμMyc*^{Tg/+};*Cry2*^{-/-} mice, whereas blood smears from control littermates did not contain detectable circulating lymphocytes (Figure S6A).

All 10-week-old *EμMyc* mice lacking CRY2 had grossly visible tumors in the mesenteric lymph nodes, whereas *EμMyc*^{Tg/+};*Cry2*^{+/+} littermates were mostly tumor-free (Figure 7D), suggesting accelerated lymphoma development in the absence of CRY2. Eventually, *EμMyc*^{Tg/+};*Cry2*^{-/-} mice succumbed earlier and with an overall greater tumor burden than *EμMyc*^{Tg/+};*Cry2*^{+/+} littermates (Figures 7D–7F and S6B). We did not detect spontaneous tumors in either wild-type or *Cry2*^{-/-} mice without the *EμMyc* transgene. Taken together, our findings indicate that CRY2 protects cells from transformation via

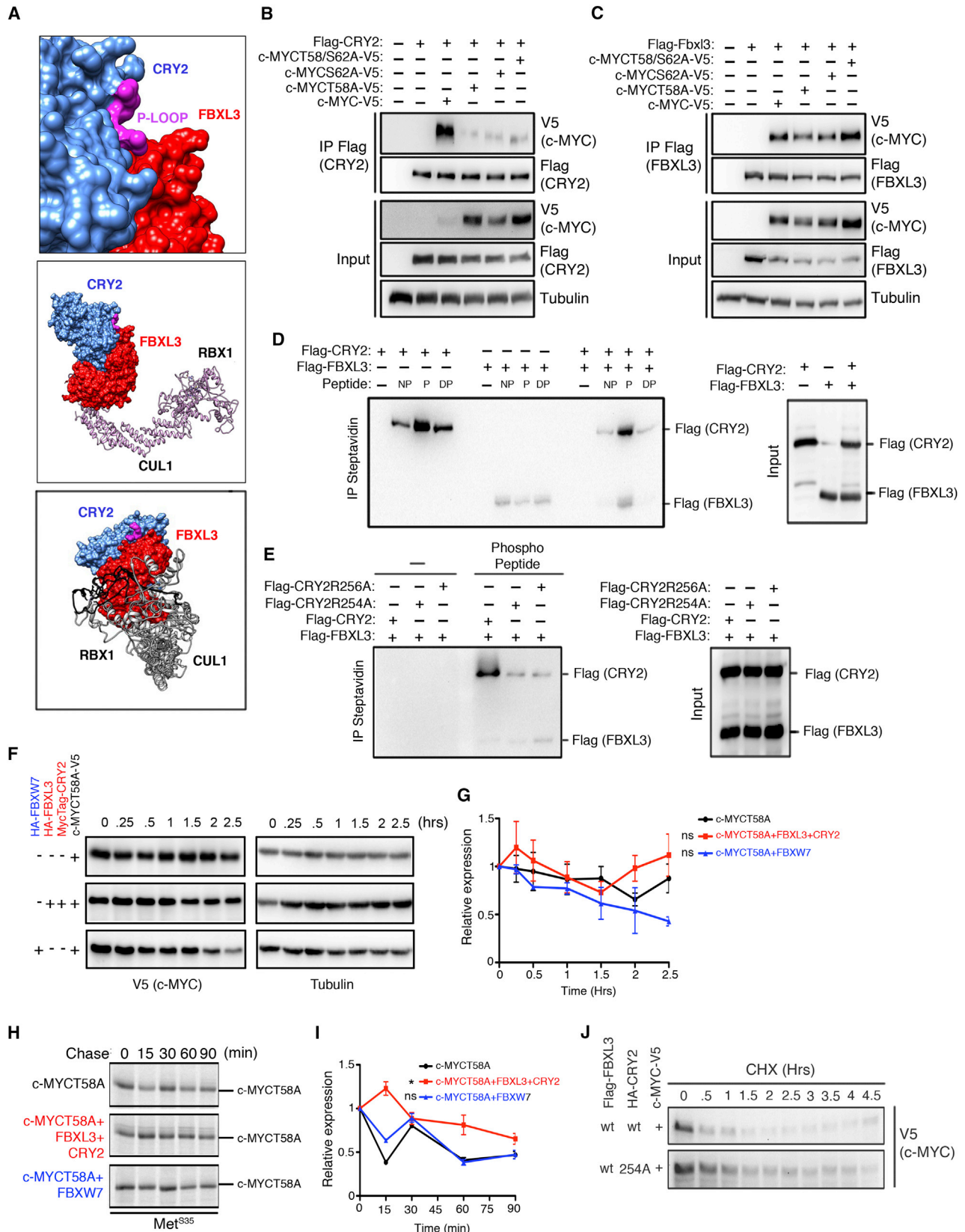
Monoclonal antibody (Mono Ab) was used to detect c-MYC (A). In (H), (J), and (L), samples from time 0 for cell lines shown in (G), (I), and (K) were loaded together for comparison. In (A), cells were treated with MG132 for 4 hr prior to lysis.

(E) Proteins detected by autoradiography after a ³⁵S-methionine pulse-chase from 293T cells expressing the indicated plasmids.

(D and F) Quantitation of the IB data (D) or the autoradiography data (F) shown in (C) and (E), respectively. Data represent the mean ± SD for triplicate samples.

*p < 0.05, **p < 0.01 versus c-MYC control by two-way ANOVA.

See also Figure S4.



(legend on next page)

pleiotropic effects, including destabilizing c-MYC via SCF^{FBXL3} and also via MYC-independent pathways to enable enhanced MYC-driven transformation in cells and in vivo (Figures 7G and 7H).

DISCUSSION

Here we report that the circadian clock component CRY2 cooperates with the E3 substrate receptor FBXL3 to degrade target proteins in a phospho-specific manner, revealing a mechanism for mammalian circadian output via CRY-driven cycles of proteasomal degradation. Our findings suggest that CRY2 and FBXL3 contribute to limiting tumor formation by promoting the turnover of c-MYC. Although CRY has never before been proposed to act as a physical component of an E3 ligase, *Drosophila melanogaster* dCRY is genetically required for light-induced degradation of dTIM via the E3 ligase JETLAG (Koh et al., 2006), suggesting that some aspects of the function that we describe here may be conserved in other systems. In addition, a recent study found that mammalian CRY1 can stimulate MDM2-driven ubiquitylation and degradation of FOXO1 (Jang et al., 2016), which may involve a related mechanism, although MDM2 is not part of an SCF complex. We anticipate that our findings will provide the basis for future identification of additional substrates recruited to SCF^{FBXL3} and/or the related CRY-binding E3 ligase SCF^{FBXL21} (Hirano et al., 2013; Yoo et al., 2013) by CRY1 and/or CRY2.

Here we describe the first demonstrated target of mammalian CRY2-dependent protein turnover: the oncoprotein c-MYC. Because the sequence surrounding c-MYC T58, which binds to CRY2, is conserved in N-MYC, L-MYC, and the c-MYC cleavage product MYC-NICK (Conacci-Sorrell et al., 2010), these may also be targeted by CRY2-SCF^{FBXL3}, although they were not examined in this study. Because ubiquitylation and proteasome activity have been shown to regulate CLOCK and BMAL1 activation of target genes (Luo et al., 2012; Stratmann et al., 2012; Tamayo et al., 2015), the novel function of CRY proteins described here may play a role in circadian clock function. Intriguingly, c-MYC can interfere with CLOCK- and BMAL1-dependent transactivation (Altman et al., 2015), so CRY2-driven MYC destabilization could reinforce circadian clock amplitude.

We recently demonstrated that CRY1 and CRY2 have divergent roles in modulating transcription in response to DNA damage (Papp et al., 2015). Reduced degradation of c-MYC in response to DNA damage could contribute to the loss of *p21*

induction in *Cry2*^{-/-} cells. The unique functions of CRY1 and CRY2 in this pathway may explain why *Cry1*^{-/-}; *Cry2*^{-/-} mice are protected from tumor development in the context of *P53* deletion (Ozturk et al., 2009) but are more susceptible to radiation-induced tumor formation (Lee et al., 2010), whereas loss of CRY2 alone enhances susceptibility to transformation in our study. Disruption of circadian rhythms likely contributes to enhanced cancer susceptibility via multiple mechanisms (Kang et al., 2010; Kemp et al., 2010; Lee et al., 2013; Lee and Sancar, 2011a, 2011b; Masri et al., 2013, 2015; Unsal-Kaçmaz et al., 2005, 2007). Indeed, the cooperation between CRY2 deficiency and multiple oncogenes in proliferation and transformation assays (Figures 1A–1G) suggests that CRY2 itself may have additional roles in suppressing these effects. The observed cooperativity between CRY2 loss and c-MYC overexpression indicates that *Cry2*^{-/-} cells harbor a defect in P19ARF and/or P53 function (Sherr, 2006, 2012). PER2 has been implicated in stabilizing P53 by opposing its MDM2-mediated ubiquitylation (Gotoh et al., 2014, 2015) and has been suggested to function as a tumor suppressor in some contexts (Chen-Goodspeed and Lee, 2007; Lee, 2006; Papagiannakopoulos et al., 2016). CRY2 deficiency could influence P19ARF/P53 by altering PER2 expression, localization, or stability. Further studies will be required to understand how the loss of CRY2 affects P53 and how PER2 and CRY2 independently and/or synergistically modulate tumor formation.

Repeated transient inactivation of c-MYC has been shown to suppress even established tumors while allowing normal tissue proliferative functions to proceed (Soucek et al., 2008, 2013); perhaps CRY2-driven circadian proteolysis of c-MYC provides analogous daily cycles of c-MYC action and degradation in a physiological context. Although c-MYC protein remains rhythmic in *Cry2*^{-/-} cells (Figures 1M and S1B), perhaps because of rhythmic mRNA expression, its elevated expression overall prevents this prolonged daily absence of c-MYC protein. Increased cancer susceptibility in shift workers and in animals subjected to circadian disruption may be in part due to elevated c-MYC driven by loss of CRY2- and FBXL3-coordinated regulation because circadian disruption would alter the dynamics of CRY2 expression. Notably, *Cry2*-deficient mice and cells maintain robust circadian rhythms (Khan et al., 2012; Thresher et al., 1998) while clearly exhibiting enhanced susceptibility to transformation, indicating that neither behavioral nor transcriptional rhythms must be globally disrupted for increased cancer susceptibility in the context of circadian disruption.

Figure 5. SCF^{FBXL3}+CRY2 Interacts Specifically with T58-Phosphorylated c-MYC

(A) Top: the P loop (magenta) at the interface of CRY2 (blue) and FBXL3 (red). Center: superposition of crystal structures from Protein Data Bank accession numbers PDB: 1LDK (SKP1-SKP2-CUL1-RBX1), 4I6J (SKP1-FBXL3-CRY2), and 4MLP (CRY2-KL001) with the CRY2 P loop highlighted in magenta. Bottom: 90° rotation of the above image.

(B and C) Proteins detected by IB following FLAG IP from 293T cells expressing the indicated plasmids.

(D and E) Proteins detected by IB following streptavidin affinity purification after incubation of purified FLAG-CRY2 and/or FLAG-FBXL3 with the indicated biotinylated peptides.

(F and J) Proteins detected by IB in whole-cell lysates from 293T cells expressing the indicated plasmids and harvested at the indicated times.

(H) Proteins detected by autoradiography after a ³⁵S-methionine pulse-chase from 293T cells expressing the indicated plasmids.

(G and I) Quantitation of the IB data (G) or the autoradiography data (I) shown in (F) and (H), respectively. Data represent the mean ± SD for triplicate samples.

**p* < 0.05 versus c-MYCT58A control by two-way ANOVA.

See also Figure S5.

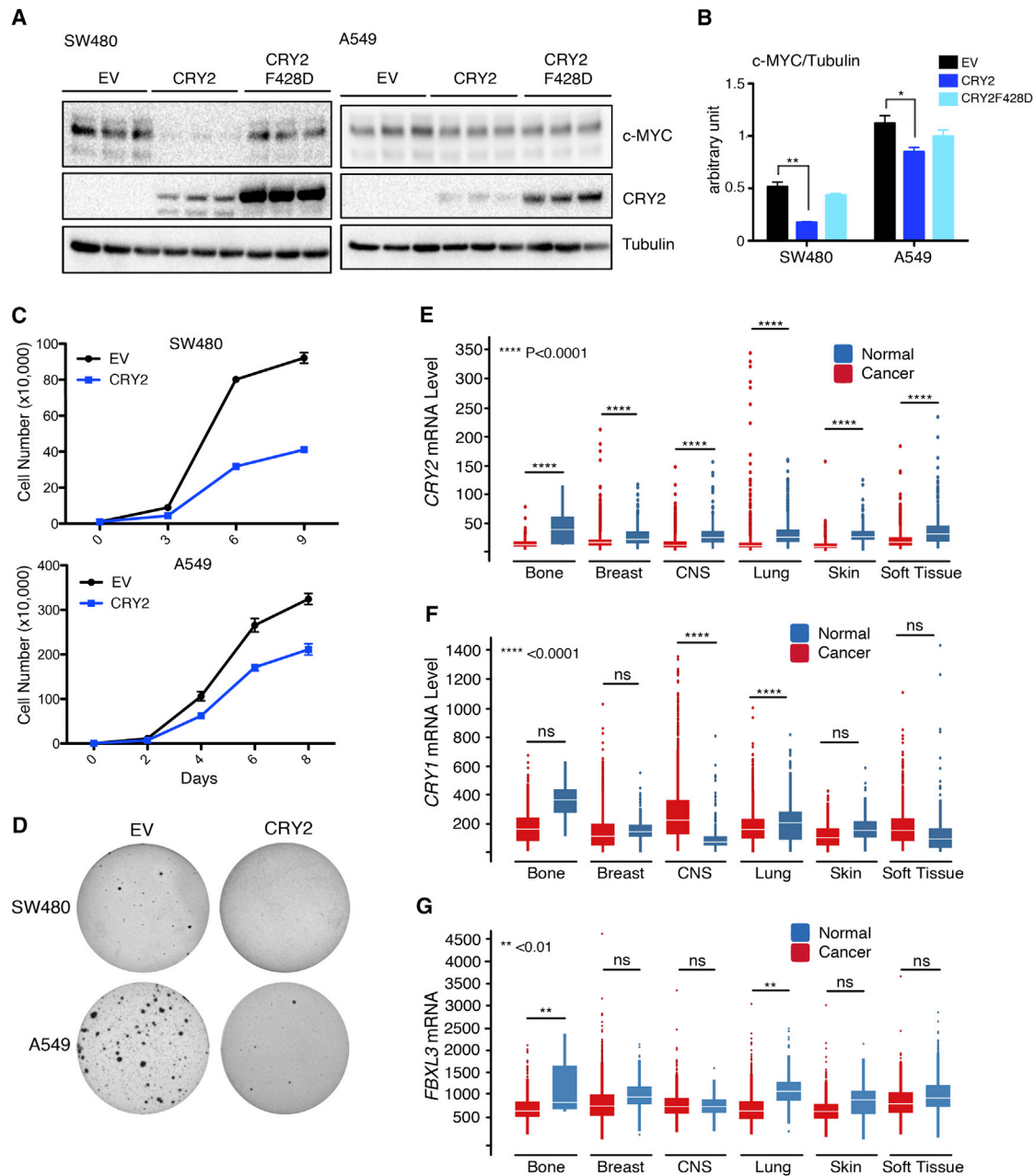


Figure 6. Low CRY2 Expression Enhances Growth of Human Cancer Cell Lines

(A, C, and D) Proteins detected by IB (A), proliferation (C), and colony formation in soft agar (D) in SW480 and A549 cells expressing the indicated plasmids. (B) Quantitation of the IB data shown in (A).

(E–G) CRY2, CRY1, and FBXL3 expression in human tumor versus normal samples.

See also Table S3.

EXPERIMENTAL PROCEDURES

Cell Culture

HEK293T (293T), A549, and SW480 cells were purchased from the American Type Culture Collection. Three different series of MEFs were isolated from embryonic day (E) 15.5 embryos. Two different series of adult skin fibroblasts were prepared from ear biopsies of adult mice of the indicated genotypes. All MEFs and adult ear fibroblasts (AEFs) were used as primary (passaged

no more than ten times and grown in 3% oxygen) or spontaneously immortalized. More detailed descriptions of all procedures are available in the [Supplemental Experimental Procedures](#).

Generation of Stable Cell Lines

Lentiviral shRNAs were produced by transient transfection in 293T cells. Beginning 48 hr after viral transduction, infected cells were cultured in selection media for 2 days to 2 weeks.

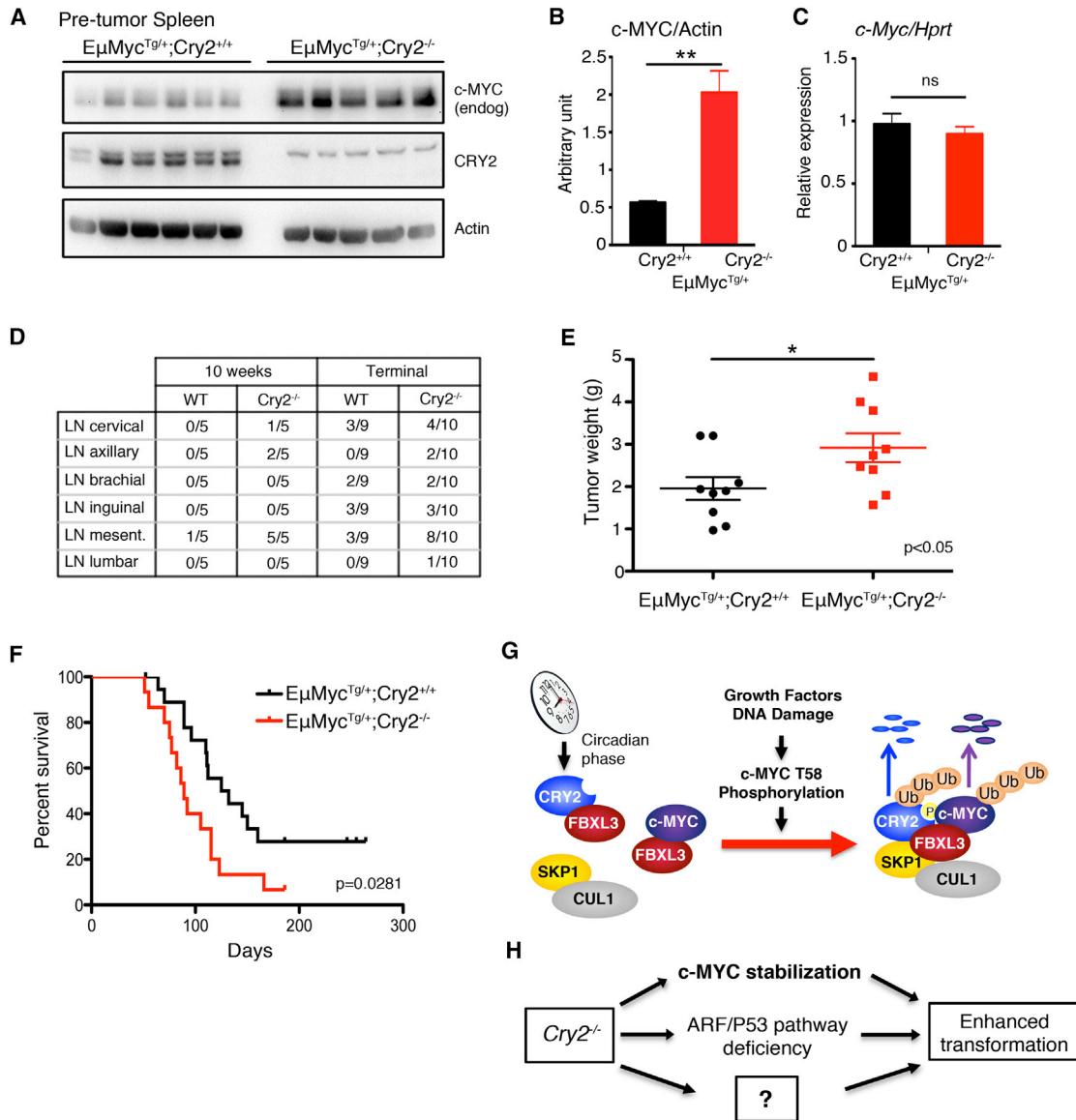


Figure 7. CRY2 Deletion Enhances MYC-Driven Lymphoma In Vivo

(A) Proteins detected by IB in spleen samples taken from 6-week-old *EμMyc^{+/+};Cry2^{+/+}* and *EμMyc^{+/+};Cry2^{-/-}* littermates.

(B) Quantitation of proteins from the western blot (WB) in (A).

(C) mRNA expression measured by qPCR in the spleen samples used in (A).

(D) Numbers of solid tumors observed in the indicated locations in *EμMyc^{+/+};Cry2^{+/+}* and *EμMyc^{+/+};Cry2^{-/-}* littermates of the indicated ages or at the time of sacrifice necessitated by advanced disease progression. LN, lymph node.

(E and F) Total combined tumor weight (E) and survival (F) at time of sacrifice because of advanced disease progression in *EμMyc^{+/+};Cry2^{+/+}* (black, n = 19) and *EμMyc^{+/+};Cry2^{-/-}* (red, n = 15) littermates.

(B and C) Data represent the mean ± SD of samples from five mice for which IB data are shown in (A).

(B and E) *p < 0.05, **p < 0.01 by t test.

(F) The p value is from log-rank calculations.

(G) Schematic for the role of CRY2 as a cofactor for SCF^{FBXL3}-driven ubiquitylation of phosphorylated c-MYC.

(H) Deletion of *Cry2* may contribute to cellular transformation in a pleiotropic manner.

See also Figure S6.

Proliferation and Transformation Assays

For proliferation analysis, cells were seeded in 6-well plates at 5,000 cells/well and counted every 2 days for 6–10 days. For colony formation, 1,000 cells were plated in 10-cm plates and grown for 2–3 weeks prior to staining.

For anchorage-independent growth, MEFs infected with virus expressing *c-MYC/shP53* were selected for 2–3 days and suspended in complete medium containing 0.4% low-melting agarose and plated in 6-well plates at a density of 20,000 cells/well onto solidified 0.8% agarose. Cells were grown for 2–3 weeks

prior to staining with 3-(4,5-dimethylthiazol-2-yl)-2,5-diphenyltetrazolium bromide (MTT).

Immunoprecipitation and western blotting were performed using standard protocols.

Pulse-Chase Labeling Experiment

Lysates from transfected 293T cells were incubated with pulse medium containing ³⁵S-methionine. The labeling was stopped by replacing the pulse medium with regular 293T cell culture medium, and cells were collected at the indicated time points.

Peptide Binding Assay

FLAG-Fbxl3 and FLAG-Cry2 were immunoprecipitated separately from transfected 293T cells and eluted with 3× FLAG peptide. After quantification, equal amounts of FLAG-Fbxl3 and/or wild-type or mutant FLAG-Cry2 were combined with biotinylated synthetic peptides as indicated and incubated at 30°C for 30 min while shaking. Streptavidin beads were added, incubated overnight at 4°C, and washed three times.

Sequential IP

Lysates from transfected 293T cells were incubated with anti-FLAG M2 agarose beads overnight at 4°C, washed three times, and incubated in 3× FLAG peptide. The elution was collected and subsequently incubated with anti-hemagglutinin (HA) agarose beads for 2 hr at 4°C. The anti-HA beads were washed three times and boiled with sample buffer.

Quantitative Real-Time PCR

RNA was extracted from MEFs using standard protocols. cDNA was prepared using QScript cDNA Supermix and analyzed for gene expression using quantitative real-time PCR with iQ SYBR Green Supermix. Primer sequences are available in the [Supplemental Experimental Procedures](#).

Isotope Labeling

Following dexamethasone-induced synchronization, cells were cultured in glucose free DMEM (Sigma) containing 15% fetal bovine serum (FBS) and 25 mM [U-¹³C₆] glucose for 10 hr. Polar metabolites and total fatty acids were extracted, derivatized, and analyzed as described previously ([Metallo et al., 2011](#); [Vacanti et al., 2014](#)).

RNA Sequencing

Reads (100 bp) were generated by the HiSeq Analyzer 2000. Genome Analyzer Pipeline software was used to perform the early data analysis. For mRNA sequencing (mRNA-seq), TopHat v2.0.13 with Bowtie2 was used to align to the mm10 genome.

GSEA

GSEA is a computational method ([Subramanian et al., 2007](#)) that determines whether an a priori defined set of genes shows statistically significant, concordant differences between two biological states (e.g., phenotypes). RNA sequencing outputs for wild-type and *Cry2*^{-/-} cells were used as input for GSEA comparing the two genotypes (wild-type versus *Cry2*^{-/-} regardless of circadian time).

Structure Modeling

Molecular graphics and analyses were performed with the University of California, San Francisco (UCSF) Chimera package ([Pettersen et al., 2004](#)). Chimera is developed by the Resource for Biocomputing, Visualization, and Informatics at UCSF (supported by the National Institute of General Medical Sciences [NIGMS] P41-GM103311).

Tissue Expression Profile

To investigate the expression profile of *CRY2* in human normal and cancer samples, publicly available microarray data were compiled, normalized, and re-analyzed by the Novartis bioinformatics group. Original data were extracted from the GEO database, CCLE database, and The Cancer Genome Atlas (TCGA) database.

Mice

Cry2^{-/-} mice were shared by Dr. Aziz Sançar ([Thresher et al., 1998](#)), and *EμMyc*^{+/-} mice ([Adams et al., 1985](#)) were purchased from The Jackson Laboratory. *Cry2*^{+/-} females were mated to *EμMyc*^{+/-} males to generate *EμMyc*^{+/-};*Cry2*^{+/-} mice. *EμMyc*^{+/-};*Cry2*^{+/-} males were mated to *Cry2*^{+/-} females to generate *EμMyc*^{+/-};*Cry2*^{+/+} and *EμMyc*^{+/-};*Cry2*^{-/-} mice used for analysis. Mice showing any signs of systemic illness were sacrificed and necropsied. All animal care and treatments were in accordance with The Scripps Research Institute guidelines for the care and use of animals and were approved by the Institutional Animal Care and Use Committee under protocol 10-0019.

Nuclear Extract from Tissue

Nuclear extracts from the spleen were prepared using the NP40, Urea, NaCl buffer (NUN) procedure as described previously ([Lavery and Schibler, 1993](#)).

Data Analysis and Statistics

All experiments were repeated at least three times, and results are presented either as one representative experiment or as an average ± SD. Statistical analyses were done using two-tailed Student's t test or with two-way ANOVA. Time-dependent survival in mouse experiments was represented with Kaplan-Meier methods, and significance was evaluated with the log-rank test.

ACCESSION NUMBERS

The accession number for the RNA sequencing data reported in this paper is GEO: GSE89018.

SUPPLEMENTAL INFORMATION

Supplemental Information includes Supplemental Experimental Procedures, six figures, and three tables and can be found with this article online at <http://dx.doi.org/10.1016/j.molcel.2016.10.012>.

AUTHOR CONTRIBUTIONS

A.L.H. performed the majority of experiments, analyzed data, made figures, and contributed to writing the paper. S.J.P., A.B.C., E.H., S.D.J., A.K., and M.N. performed experiments. M.W. and C.M.M. designed, performed, and supervised metabolic labeling experiments and analysis. Z.L. performed bioinformatics analyses (Tables S1 and S3; Figures 6D–6F). K.A.L. conceived and supervised the study, performed structural modeling and GSEA, analyzed data, made figures, and wrote the paper. All authors edited and approved the manuscript.

ACKNOWLEDGMENTS

This work was supported by grants from the NIH to K.A.L. (DK090188 and DK097164) and C.M.M. (CA188652), Searle Scholars awards to K.A.L. and C.M.M. from the Kinship Foundation, a cancer research scholar award to K.A.L. from the Sidney Kimmel Cancer Research Foundation, a grant to K.A.L. from the Lung Cancer Research Foundation, and by fellowships from the Swedish Research Council to E.H. and the Deutsche Forschungsgemeinschaft and American Heart Association (15POST22510020) to S.D.J. Chimera is developed by the Resource for Biocomputing, Visualization, and Informatics at UCSF (supported by NIGMS P41-GM103311). We thank Reuben Shaw, Clodagh O'Shea, Michael Hemann, Thales Papagiannakopoulos, Luke Wiseman, Eric Bennett, Brenda Schulman, Daniel Scott, Megan Afetian, Drew Duglan, Megan Vaughan, Colby Sandate, Jamie Williamson, Michael and Louise McHeyzer-Williams, and Eros Lazzarini-Denchi for helpful discussions, sharing reagents or equipment, and/or critical reading of the manuscript.

Received: March 14, 2016

Revised: August 31, 2016

Accepted: October 6, 2016

Published: November 10, 2016

REFERENCES

- Adams, J.M., Harris, A.W., Pinkert, C.A., Corcoran, L.M., Alexander, W.S., Cory, S., Palmiter, R.D., and Brinster, R.L. (1985). The c-myc oncogene driven by immunoglobulin enhancers induces lymphoid malignancy in transgenic mice. *Nature* **318**, 533–538.
- Altman, B.J., Hsieh, A.L., Sengupta, A., Krishnanaiah, S.Y., Stine, Z.E., Walton, Z.E., Gouw, A.M., Venkataraman, A., Li, B., Goraksha-Hicks, P., et al. (2015). MYC disrupts the circadian clock and metabolism in cancer cells. *Cell Metab.* **22**, 1009–1019.
- Balsalobre, A., Brown, S.A., Marcacci, L., Tronche, F., Kellendonk, C., Reichardt, H.M., Schütz, G., and Schibler, U. (2000). Resetting of circadian time in peripheral tissues by glucocorticoid signaling. *Science* **289**, 2344–2347.
- Bhatia, K., Huppi, K., Spangler, G., Siwarski, D., Iyer, R., and Magrath, I. (1993). Point mutations in the c-Myc transactivation domain are common in Burkitt's lymphoma and mouse plasmacytomas. *Nat. Genet.* **5**, 56–61.
- Bhatia, K., Spangler, G., Gaidano, G., Hamdy, N., Dalla-Favera, R., and Magrath, I. (1994). Mutations in the coding region of c-myc occur frequently in acquired immunodeficiency syndrome-associated lymphomas. *Blood* **84**, 883–888.
- Busino, L., Bassermann, F., Maiolica, A., Lee, C., Nolan, P.M., Godinho, S.I., Draetta, G.F., and Pagano, M. (2007). SCFFbx13 controls the oscillation of the circadian clock by directing the degradation of cryptochrome proteins. *Science* **316**, 900–904.
- Chakraborty, A.A., and Tansey, W.P. (2009). Inference of cell cycle-dependent proteolysis by laser scanning cytometry. *Exp. Cell Res.* **315**, 1772–1778.
- Chen-Goodspeed, M., and Lee, C.C. (2007). Tumor suppression and circadian function. *J. Biol. Rhythms* **22**, 291–298.
- Conacci-Sorrell, M., Ngouenet, C., and Eisenman, R.N. (2010). Myc-nick: a cytoplasmic cleavage product of Myc that promotes alpha-tubulin acetylation and cell differentiation. *Cell* **142**, 480–493.
- Farrell, A.S., and Sears, R.C. (2014). MYC degradation. *Cold Spring Harb. Perspect. Med.* **4**, 4.
- Fu, L., and Kettner, N.M. (2013). The circadian clock in cancer development and therapy. *Prog. Mol. Biol. Transl. Sci.* **119**, 221–282.
- Fu, L., Pelicano, H., Liu, J., Huang, P., and Lee, C. (2002). The circadian gene *Period2* plays an important role in tumor suppression and DNA damage response in vivo. *Cell* **111**, 41–50.
- Gaddameedhi, S., Selby, C.P., Kaufmann, W.K., Smart, R.C., and Sancar, A. (2011). Control of skin cancer by the circadian rhythm. *Proc. Natl. Acad. Sci. USA* **108**, 18790–18795.
- Geyfman, M., Kumar, V., Liu, Q., Ruiz, R., Gordon, W., Espitia, F., Cam, E., Millar, S.E., Smyth, P., Ihler, A., et al. (2012). Brain and muscle Arnt-like protein-1 (BMAL1) controls circadian cell proliferation and susceptibility to UVB-induced DNA damage in the epidermis. *Proc. Natl. Acad. Sci. USA* **109**, 11758–11763.
- Godinho, S.I., Maywood, E.S., Shaw, L., Tucci, V., Barnard, A.R., Busino, L., Pagano, M., Kendall, R., Quwailid, M.M., Romero, M.R., et al. (2007). The after-hours mutant reveals a role for Fbx13 in determining mammalian circadian period. *Science* **316**, 897–900.
- Gotoh, T., Vila-Caballer, M., Santos, C.S., Liu, J., Yang, J., and Finkielstein, C.V. (2014). The circadian factor *Period 2* modulates p53 stability and transcriptional activity in unstressed cells. *Mol. Biol. Cell* **25**, 3081–3093.
- Gotoh, T., Vila-Caballer, M., Liu, J., Schiffhauer, S., and Finkielstein, C.V. (2015). Association of the circadian factor *Period 2* to p53 influences p53's function in DNA-damage signaling. *Mol. Biol. Cell* **26**, 359–372.
- Gregory, M.A., Qi, Y., and Hann, S.R. (2003). Phosphorylation by glycogen synthase kinase-3 controls c-myc proteolysis and subnuclear localization. *J. Biol. Chem.* **278**, 51606–51612.
- Hao, B., Zheng, N., Schulman, B.A., Wu, G., Miller, J.J., Pagano, M., and Pavletich, N.P. (2005). Structural basis of the Cks1-dependent recognition of p27(Kip1) by the SCF(Skp2) ubiquitin ligase. *Mol. Cell* **20**, 9–19.
- Hao, B., Oehlmann, S., Sowa, M.E., Harper, J.W., and Pavletich, N.P. (2007). Structure of a Fbw7-Skp1-cyclin E complex: multisite-phosphorylated substrate recognition by SCF ubiquitin ligases. *Mol. Cell* **26**, 131–143.
- Hirano, A., Yumimoto, K., Tsunematsu, R., Matsumoto, M., Oyama, M., Kozuka-Hata, H., Nakagawa, T., Lanjakornsiripan, D., Nakayama, K.I., and Fukada, Y. (2013). FBXL21 regulates oscillation of the circadian clock through ubiquitination and stabilization of cryptochromes. *Cell* **152**, 1106–1118.
- Hitomi, K., DiTacchio, L., Arvai, A.S., Yamamoto, J., Kim, S.T., Todo, T., Tainer, J.A., Iwai, S., Panda, S., and Getzoff, E.D. (2009). Functional motifs in the (6–4) photolyase crystal structure make a comparative framework for DNA repair photolyases and clock cryptochromes. *Proc. Natl. Acad. Sci. USA* **106**, 6962–6967.
- Jang, H., Lee, G.Y., Selby, C.P., Lee, G., Jeon, Y.G., Lee, J.H., Cheng, K.K., Titchenell, P., Birnbaum, M.J., Xu, A., et al. (2016). SREBP1c-CRY1 signalling represses hepatic glucose production by promoting FOXO1 degradation during refeeding. *Nat. Commun.* **7**, 12180.
- Janich, P., Pascual, G., Merlos-Suárez, A., Battle, E., Ripperger, J., Albrecht, U., Cheng, H.Y., Obrietan, K., Di Croce, L., and Benitah, S.A. (2011). The circadian molecular clock creates epidermal stem cell heterogeneity. *Nature* **480**, 209–214.
- Kang, T.H., Lindsey-Boltz, L.A., Reardon, J.T., and Sancar, A. (2010). Circadian control of XPA and excision repair of cisplatin-DNA damage by cryptochrome and HERC2 ubiquitin ligase. *Proc. Natl. Acad. Sci. USA* **107**, 4890–4895.
- Kemp, M.G., Akan, Z., Yilmaz, S., Grillo, M., Smith-Roe, S.L., Kang, T.H., Cordeiro-Stone, M., Kaufmann, W.K., Abraham, R.T., Sancar, A., and Unsal-Kaçmaz, K. (2010). Tipin-replication protein A interaction mediates Chk1 phosphorylation by ATR in response to genotoxic stress. *J. Biol. Chem.* **285**, 16562–16571.
- Khan, S.K., Xu, H., Ukai-Tadenuma, M., Burton, B., Wang, Y., Ueda, H.R., and Liu, A.C. (2012). Identification of a novel cryptochrome differentiating domain required for feedback repression in circadian clock function. *J. Biol. Chem.* **287**, 25917–25926.
- Koh, K., Zheng, X., and Sehgal, A. (2006). JETLAG resets the *Drosophila* circadian clock by promoting light-induced degradation of TIMELESS. *Science* **312**, 1809–1812.
- Koike, N., Yoo, S.H., Huang, H.C., Kumar, V., Lee, C., Kim, T.K., and Takahashi, J.S. (2012). Transcriptional architecture and chromatin landscape of the core circadian clock in mammals. *Science* **338**, 349–354.
- Lavery, D.J., and Schibler, U. (1993). Circadian transcription of the cholesterol 7 alpha hydroxylase gene may involve the liver-enriched bZIP protein DBP. *Genes Dev.* **7**, 1871–1884.
- Lee, C.C. (2006). Tumor suppression by the mammalian *Period* genes. *Cancer Causes Control* **17**, 525–530.
- Lee, J.H., and Sancar, A. (2011a). Circadian clock disruption improves the efficacy of chemotherapy through p73-mediated apoptosis. *Proc. Natl. Acad. Sci. USA* **108**, 10668–10672.
- Lee, J.H., and Sancar, A. (2011b). Regulation of apoptosis by the circadian clock through NF-kappaB signaling. *Proc. Natl. Acad. Sci. USA* **108**, 12036–12041.
- Lee, S., Donehower, L.A., Herron, A.J., Moore, D.D., and Fu, L. (2010). Disrupting circadian homeostasis of sympathetic signaling promotes tumor development in mice. *PLoS ONE* **5**, e10995.
- Lee, J.H., Gaddameedhi, S., Ozturk, N., Ye, R., and Sancar, A. (2013). DNA damage-specific control of cell death by cryptochrome in p53-mutant ras-transformed cells. *Cancer Res.* **73**, 785–791.
- Liberzon, A., Birger, C., Thorvaldsdóttir, H., Ghandi, M., Mesirov, J.P., and Tamayo, P. (2015). The Molecular Signatures Database (MSigDB) hallmark gene set collection. *Cell Syst.* **1**, 417–425.
- Lin, C.Y., Lovén, J., Rahl, P.B., Paranal, R.M., Burge, C.B., Bradner, J.E., Lee, T.I., and Young, R.A. (2012). Transcriptional amplification in tumor cells with elevated c-Myc. *Cell* **151**, 56–67.

- Luo, W., Li, Y., Tang, C.H., Abruzzi, K.C., Rodriguez, J., Pescatore, S., and Rosbash, M. (2012). CLOCK deubiquitylation by USP8 inhibits CLK/CYC transcription in *Drosophila*. *Genes Dev.* 26, 2536–2549.
- Malempati, S., Tibbitts, D., Cunningham, M., Akkari, Y., Olson, S., Fan, G., and Sears, R.C. (2006). Aberrant stabilization of c-Myc protein in some lymphoblastic leukemias. *Leukemia* 20, 1572–1581.
- Masri, S., Cervantes, M., and Sassone-Corsi, P. (2013). The circadian clock and cell cycle: interconnected biological circuits. *Curr. Opin. Cell Biol.* 25, 730–734.
- Masri, S., Kinouchi, K., and Sassone-Corsi, P. (2015). Circadian clocks, epigenetics, and cancer. *Curr. Opin. Oncol.* 27, 50–56.
- Metallo, C.M., Gameiro, P.A., Bell, E.L., Mattaini, K.R., Yang, J., Hiller, K., Jewell, C.M., Johnson, Z.R., Irvine, D.J., Guarente, L., et al. (2011). Reductive glutamine metabolism by IDH1 mediates lipogenesis under hypoxia. *Nature* 481, 380–384.
- Nangle, S., Xing, W., and Zheng, N. (2013). Crystal structure of mammalian cryptochrome in complex with a small molecule competitor of its ubiquitin ligase. *Cell Res.* 23, 1417–1419.
- Nie, Z., Hu, G., Wei, G., Cui, K., Yamane, A., Resch, W., Wang, R., Green, D.R., Tessarollo, L., Casellas, R., et al. (2012). c-Myc is a universal amplifier of expressed genes in lymphocytes and embryonic stem cells. *Cell* 151, 68–79.
- Ozturk, N., Lee, J.H., Gaddameedhi, S., and Sancar, A. (2009). Loss of cryptochrome reduces cancer risk in p53 mutant mice. *Proc. Natl. Acad. Sci. USA* 106, 2841–2846.
- Panda, S., Antoch, M.P., Miller, B.H., Su, A.I., Schook, A.B., Straume, M., Schultz, P.G., Kay, S.A., Takahashi, J.S., and Hogenesch, J.B. (2002). Coordinated transcription of key pathways in the mouse by the circadian clock. *Cell* 109, 307–320.
- Papagiannakopoulos, T., Bauer, M.R., Davidson, S.M., Heimann, M., Subbaraj, L., Bhutkar, A., Bartlebaugh, J., Vander Heiden, M.G., and Jacks, T. (2016). Circadian rhythm disruption promotes lung tumorigenesis. *Cell Metab.* 24, 324–331.
- Papp, S.J., Huber, A.L., Jordan, S.D., Kriebs, A., Nguyen, M., Moresco, J.J., Yates, J.R., and Lamia, K.A. (2015). DNA damage shifts circadian clock time via Hausp-dependent Cry1 stabilization. *eLife* 4, 4.
- Partch, C.L., Green, C.B., and Takahashi, J.S. (2014). Molecular architecture of the mammalian circadian clock. *Trends Cell Biol.* 24, 90–99.
- Petterson, E.F., Goddard, T.D., Huang, C.C., Couch, G.S., Greenblatt, D.M., Meng, E.C., and Ferrin, T.E. (2004). UCSF Chimera—a visualization system for exploratory research and analysis. *J. Comput. Chem.* 25, 1605–1612.
- Popov, N., Herold, S., Llamazares, M., Schüle, C., and Eilers, M. (2007). Fbw7 and Usp28 regulate myc protein stability in response to DNA damage. *Cell Cycle* 6, 2327–2331.
- Sabò, A., Kress, T.R., Pelizzola, M., de Pretis, S., Gorski, M.M., Tesi, A., Morelli, M.J., Bora, P., Doni, M., Verrecchia, A., et al. (2014). Selective transcriptional regulation by Myc in cellular growth control and lymphomagenesis. *Nature* 511, 488–492.
- Salghetti, S.E., Kim, S.Y., and Tansey, W.P. (1999). Destruction of Myc by ubiquitin-mediated proteolysis: cancer-associated and transforming mutations stabilize Myc. *EMBO J.* 18, 717–726.
- Sherr, C.J. (2006). Divorcing ARF and p53: an unsettled case. *Nat. Rev. Cancer* 6, 663–673.
- Sherr, C.J. (2012). Ink4-Arf locus in cancer and aging. *Wiley Interdiscip. Rev. Dev. Biol.* 1, 731–741.
- Siepkka, S.M., Yoo, S.H., Park, J., Song, W., Kumar, V., Hu, Y., Lee, C., and Takahashi, J.S. (2007). Circadian mutant Overtime reveals F-box protein FBXL3 regulation of cryptochrome and period gene expression. *Cell* 129, 1011–1023.
- Soucek, L., Whitfield, J., Martins, C.P., Finch, A.J., Murphy, D.J., Sodik, N.M., Karnezis, A.N., Swigart, L.B., Nasi, S., and Evan, G.I. (2008). Modelling Myc inhibition as a cancer therapy. *Nature* 455, 679–683.
- Soucek, L., Whitfield, J.R., Sodik, N.M., Massó-Vallés, D., Serrano, E., Karnezis, A.N., Swigart, L.B., and Evan, G.I. (2013). Inhibition of Myc family proteins eradicates KRas-driven lung cancer in mice. *Genes Dev.* 27, 504–513.
- Storch, K.F., Lipan, O., Leykin, I., Viswanathan, N., Davis, F.C., Wong, W.H., and Weitz, C.J. (2002). Extensive and divergent circadian gene expression in liver and heart. *Nature* 417, 78–83.
- Straif, K., Baan, R., Grosse, Y., Secretan, B., El Ghissassi, F., Bouvard, V., Altieri, A., Benbrahim-Tallaa, L., and Coglian, V.; WHO International Agency For Research on Cancer Monograph Working Group (2007). Carcinogenicity of shift-work, painting, and fire-fighting. *Lancet Oncol.* 8, 1065–1066.
- Stratmann, M., Suter, D.M., Molina, N., Naef, F., and Schibler, U. (2012). Circadian Dbp transcription relies on highly dynamic BMAL1-CLOCK interaction with E boxes and requires the proteasome. *Mol. Cell* 48, 277–287.
- Subramanian, A., Kuehn, H., Gould, J., Tamayo, P., and Mesirov, J.P. (2007). GSEA-P: a desktop application for gene set enrichment analysis. *Bioinformatics* 23, 3251–3253.
- Tamayo, A.G., Duong, H.A., Robles, M.S., Mann, M., and Weitz, C.J. (2015). Histone monoubiquitination by Clock-Bmal1 complex marks Per1 and Per2 genes for circadian feedback. *Nat. Struct. Mol. Biol.* 22, 759–766.
- Thomas, L.R., and Tansey, W.P. (2011). Proteolytic control of the oncoprotein transcription factor Myc. *Adv. Cancer Res.* 110, 77–106.
- Thresher, R.J., Vitaterna, M.H., Miyamoto, Y., Kazantsev, A., Hsu, D.S., Petit, C., Selby, C.P., Dawut, L., Smithies, O., Takahashi, J.S., and Sancar, A. (1998). Role of mouse cryptochrome blue-light photoreceptor in circadian photoreponses. *Science* 282, 1490–1494.
- Ukai-Tadenuma, M., Yamada, R.G., Xu, H., Ripberger, J.A., Liu, A.C., and Ueda, H.R. (2011). Delay in feedback repression by cryptochrome 1 is required for circadian clock function. *Cell* 144, 268–281.
- Unsal-Kaçmaz, K., Mullen, T.E., Kaufmann, W.K., and Sancar, A. (2005). Coupling of human circadian and cell cycles by the timeless protein. *Mol. Cell Biol.* 25, 3109–3116.
- Unsal-Kaçmaz, K., Chastain, P.D., Qu, P.P., Minoo, P., Cordeiro-Stone, M., Sancar, A., and Kaufmann, W.K. (2007). The human Tim/Tipin complex coordinates an Intra-S checkpoint response to UV that slows replication fork displacement. *Mol. Cell Biol.* 27, 3131–3142.
- Vacanti, N.M., Divakaruni, A.S., Green, C.R., Parker, S.J., Henry, R.R., Ciaraldi, T.P., Murphy, A.N., and Metallo, C.M. (2014). Regulation of substrate utilization by the mitochondrial pyruvate carrier. *Mol. Cell* 56, 425–435.
- Van Dycke, K.C., Rodenburg, W., van Oostrom, C.T., van Kerkhof, L.W., Pennings, J.L., Roenneberg, T., van Steeg, H., and van der Horst, G.T. (2015). Chronically alternating light cycles increase breast cancer risk in mice. *Curr. Biol.* 25, 1932–1937.
- Walz, S., Lorenzin, F., Morton, J., Wiese, K.E., von Eyss, B., Herold, S., Rycak, L., Dumay-Odelot, H., Karim, S., Bartkuhn, M., et al. (2014). Activation and repression by oncogenic MYC shape tumour-specific gene expression profiles. *Nature* 511, 483–487.
- Welcker, M., and Clurman, B.E. (2008). FBW7 ubiquitin ligase: a tumour suppressor at the crossroads of cell division, growth and differentiation. *Nat. Rev. Cancer* 8, 83–93.
- Welcker, M., Orian, A., Jin, J., Grim, J.E., Harper, J.W., Eisenman, R.N., and Clurman, B.E. (2004). The Fbw7 tumor suppressor regulates glycogen synthase kinase 3 phosphorylation-dependent c-Myc protein degradation. *Proc. Natl. Acad. Sci. USA* 101, 9085–9090.
- West, A.C., and Bechtold, D.A. (2015). The cost of circadian desynchrony: evidence, insights and open questions. *BioEssays* 37, 777–788.
- Xing, W., Busino, L., Hinds, T.R., Mariotti, S.T., Saifee, N.H., Bush, M.F., Pagano, M., and Zheng, N. (2013). SCF(FBXL3) ubiquitin ligase targets cryptochromes at their cofactor pocket. *Nature* 496, 64–68.
- Yada, M., Hatakeyama, S., Kamura, T., Nishiyama, M., Tsunematsu, R., Imaki, H., Ishida, N., Okumura, F., Nakayama, K., and Nakayama, K.I. (2004). Phosphorylation-dependent degradation of c-Myc is mediated by the F-box protein Fbw7. *EMBO J.* 23, 2116–2125.

Yoo, S.H., Mohawk, J.A., Slepka, S.M., Shan, Y., Huh, S.K., Hong, H.K., Kornblum, I., Kumar, V., Koike, N., Xu, M., et al. (2013). Competing E3 ubiquitin ligases govern circadian periodicity by degradation of CRY in nucleus and cytoplasm. *Cell* *152*, 1091–1105.

Yumimoto, K., Matsumoto, M., Oyamada, K., Moroishi, T., and Nakayama, K.I. (2012). Comprehensive identification of substrates for F-box proteins by differential proteomics analysis. *J. Proteome Res.* *11*, 3175–3185.

Yumimoto, K., Muneoka, T., Tsuboi, T., and Nakayama, K.I. (2013). Substrate binding promotes formation of the Skp1-Cul1-Fbxl3 (SCF(Fbxl3)) protein complex. *J. Biol. Chem.* *288*, 32766–32776.

Zheng, N., Schulman, B.A., Song, L., Miller, J.J., Jeffrey, P.D., Wang, P., Chu, C., Koepp, D.M., Elledge, S.J., Pagano, M., et al. (2002). Structure of the Cul1-Rbx1-Skp1-F boxSkp2 SCF ubiquitin ligase complex. *Nature* *416*, 703–709.

Molecular Cell, Volume 64

Supplemental Information

CRY2 and FBXL3 Cooperatively Degrade c-MYC

Anne-Laure Huber, Stephanie J. Papp, Alanna B. Chan, Emma Henriksson, Sabine D. Jordan, Anna Kriebs, Madelena Nguyen, Martina Wallace, Zhizhong Li, Christian M. Metallo, and Katja A. Lamia

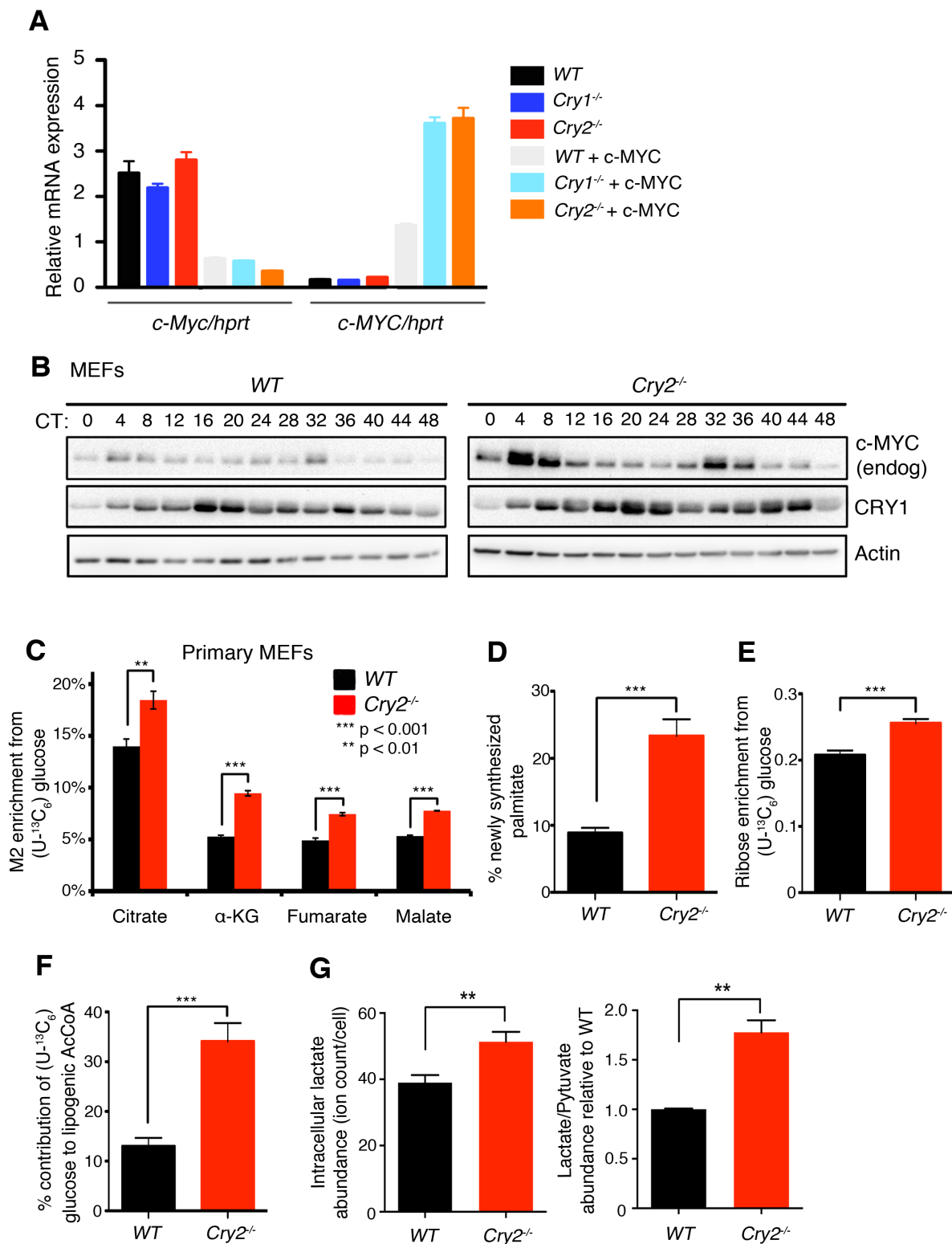


Figure S1. Related to Figure 1. CRY2 deletion enhances cell growth and transformation

(A) mRNA measured by qPCR from MEFs of the indicated genotypes stably overexpressing c-MYC. (B) Endogenous proteins detected by IB in MEFs of the indicated genotypes and harvested at the indicated times (CT: hours after circadian synchronization). (C-G) Isotope incorporation from [U-¹³C₆]-glucose into Krebs intermediates and ribose, and % newly synthesized palmitate determined by isotopomer spectral analysis (ISA) in primary MEFs. In (C-G), data represent the mean ± s.d. N≥3. **P<0.01, ***P < 0.001 by t-test

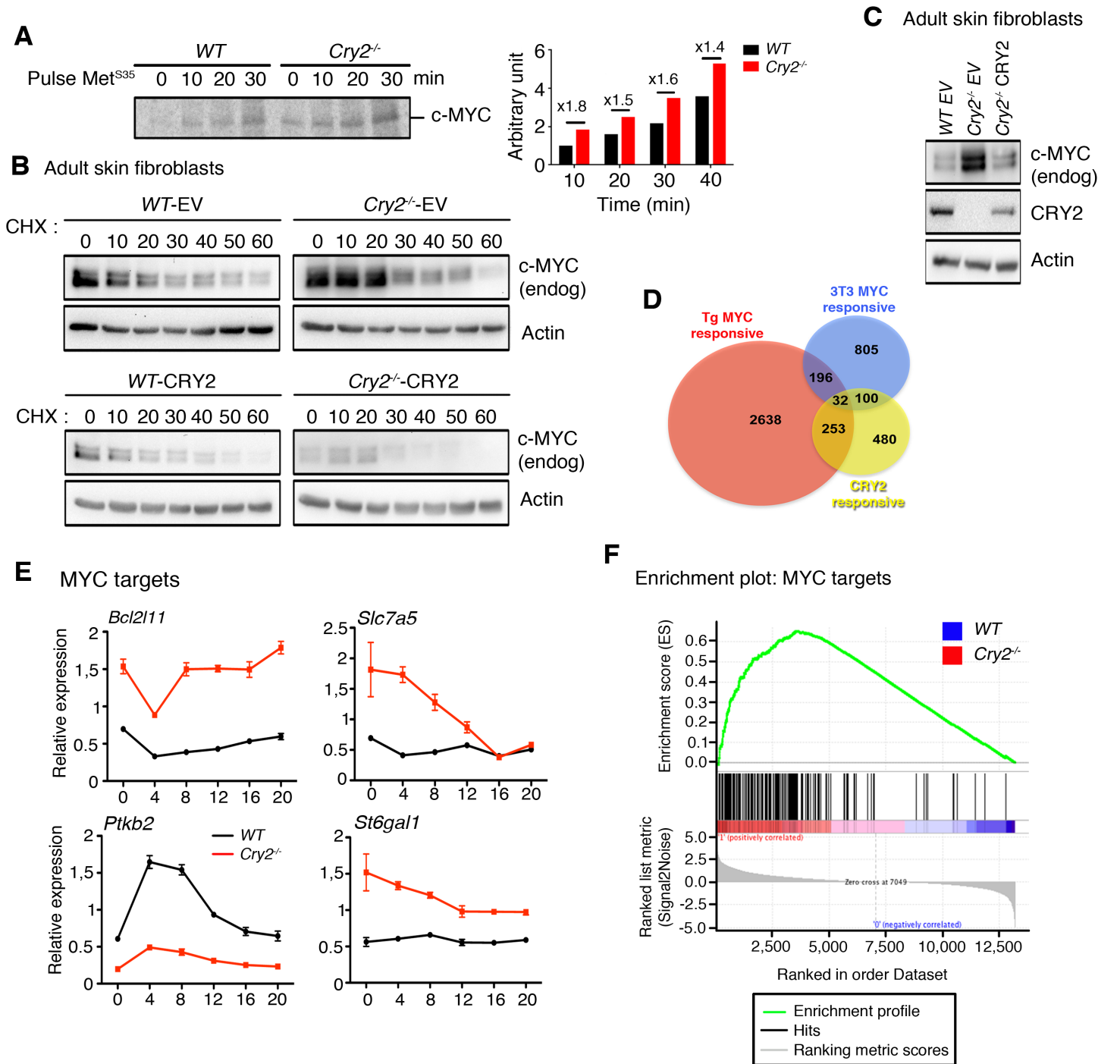


Figure S2. Related to Figure 2. CRY2 deletion increases c-MYC stability

(A) Proteins detected by autoradiography after a ³⁵S Met Pulse following c-MYC IP in adult skin fibroblasts of the indicated genotypes. (B,C) Endogenous proteins detected by IB in adult skin fibroblasts of the indicated genotypes expressing the indicated plasmids and harvested at the indicated times (CHX: minutes after cycloheximide). (C) Samples from time 0 for cell lines shown in (B) loaded together. (D) Venn diagram showing overlap of genes for which expression is significantly altered (FDR < 0.01) by genetic deletion of *Cry2* in MEFs (yellow) and those that are both responsive to increased MYC expression and harbor MYC bound to the promoter either in transgenic mice (red) or in 3T3 fibroblasts expressing a tamoxifen-inducible MYC (blue). Data for MYC responsive and MYC-bound genes were extracted from Sabo et al. (2014). (E) Transcripts measured by qPCR in wildtype (black) and *Cry2*^{-/-} (red) primary MEFs after circadian synchronization. Data represent the mean ± s.d. for three biological replicates each measured in triplicate. (F) GSEA Enrichment Plot: The top portion shows the running enrichment score (ES) for the gene set as the analysis walks down the ranked list. The middle portion shows where the members of the gene set appear in the ranked list of genes. The bottom portion shows the value of the ranking metric as you move down the list of ranked genes. The ranking metric measures a gene's correlation with a phenotype.

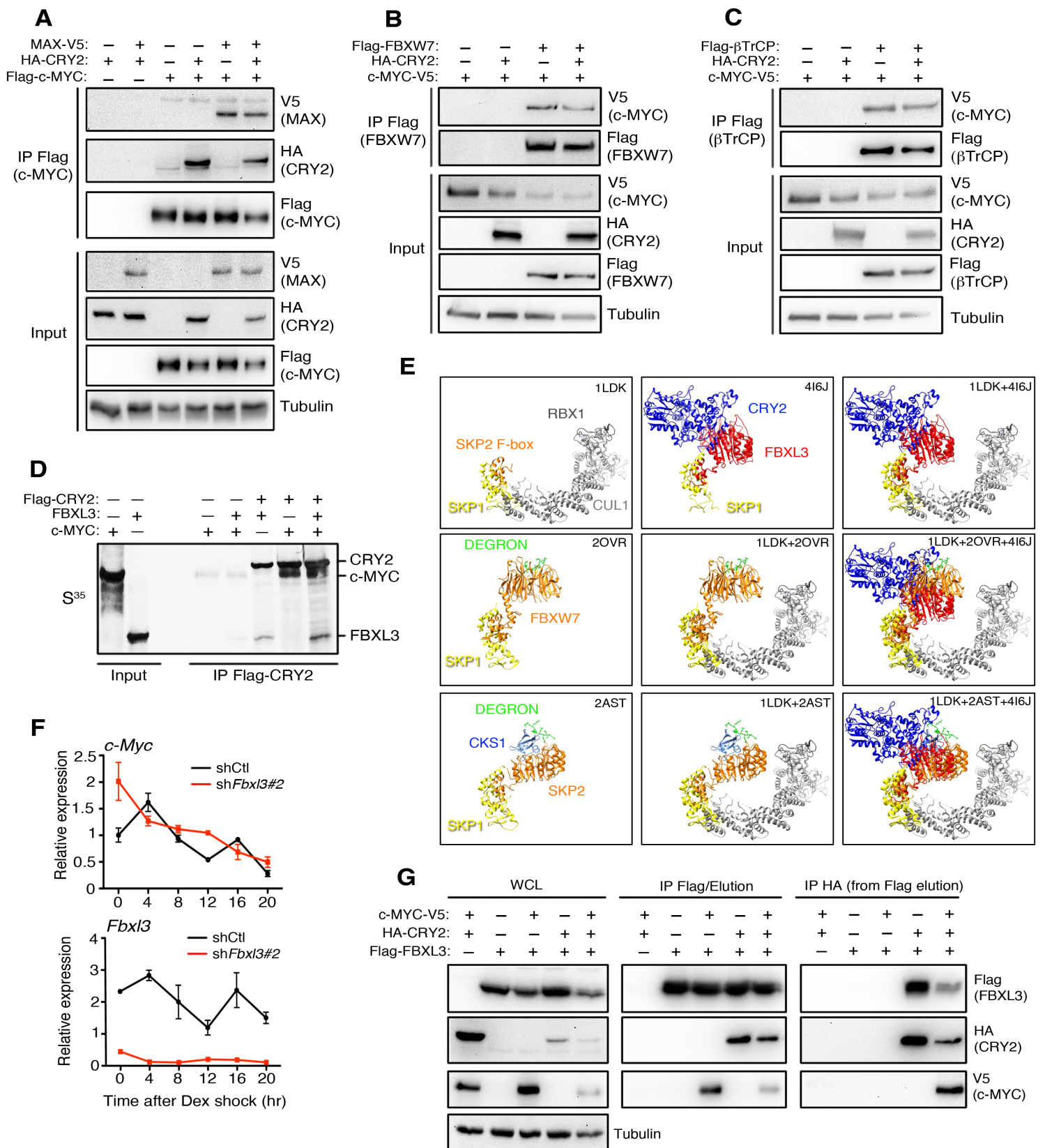


Figure S3. Related to Figure 3. c-MYC forms a complex with CRY2 and FBXL3

(A-C, G) Proteins detected by IB following FLAG or HA IP from lysates of 293T cells expressing the indicated plasmids. (D) Film detection of ³⁵S-labeled proteins detected in input or FLAG IPs from combinations of the indicated proteins produced by in vitro transcription and translation in rabbit reticulocyte lysates. (E) Individual or superimposed crystal structures from Protein Data Bank accession numbers 1LDK (SKP1-SKP2-CUL1-RBX1), 2OVR (SKP1-FBW7-CYCEDegN), 2AST (SKP1-SKP2-CKS1-p27KIP1), and 4I6J (SKP1-FBXL3-CRY2). (F) Transcripts measured by qPCR in primary MEFs expressing the indicated shRNA at the indicated times after circadian synchronization with dexamethasone. In (F) data represent the mean ± s.d. for three biological replicates each measured in triplicate.

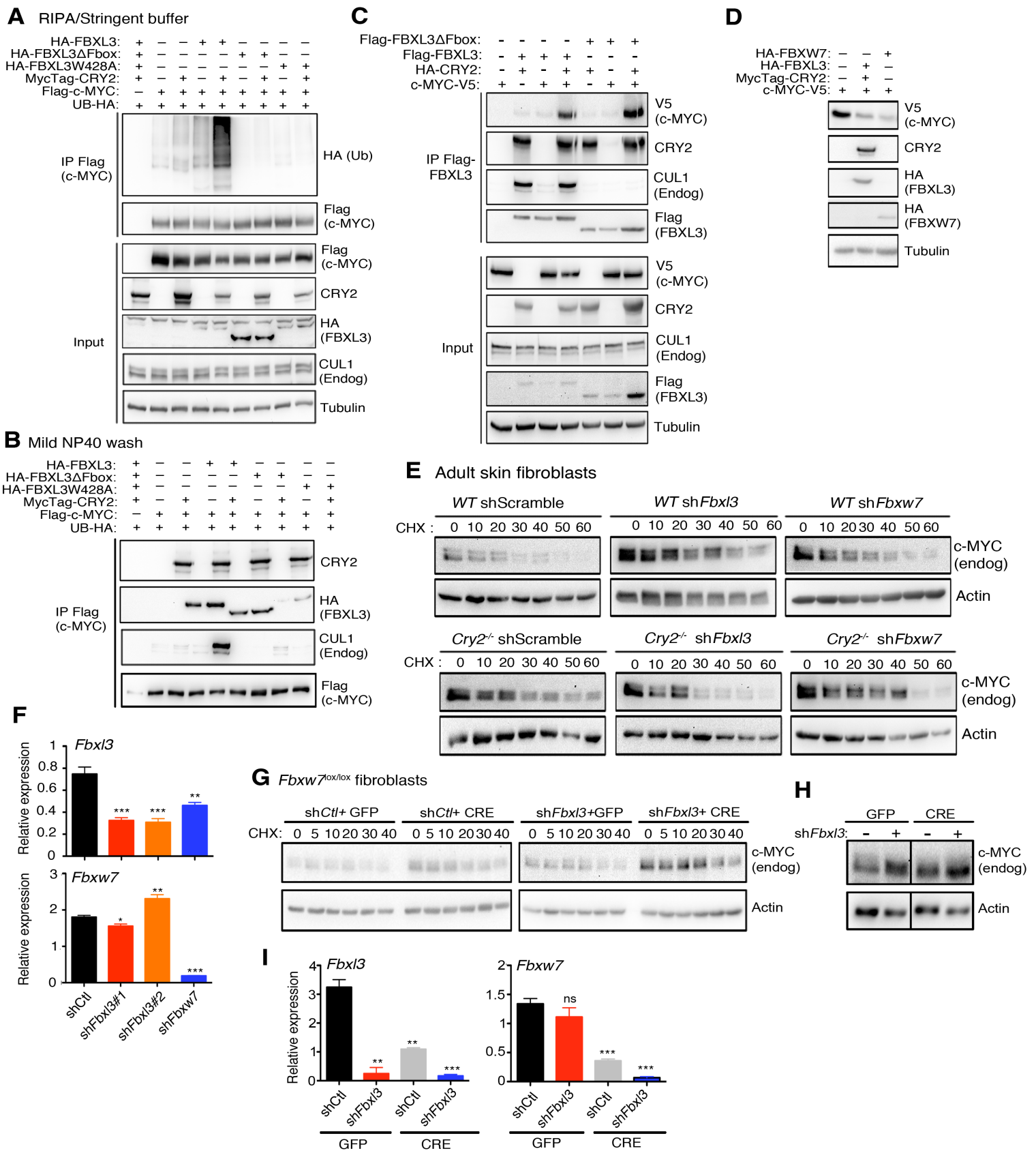


Figure S4. Related to Figure 4. CRY2 is an essential component of SCF^{FBXL3}-driven c-MYC ubiquitylation

(A,B) Proteins detected by IB following FLAG IP from 293T cells expressing the indicated plasmids. IP samples were split in half and washed with a stringent washing buffer (A) or with a mild washing buffer (B). In (A,B) cells were treated with MG132 for 6 hours prior to lysis. (C) Proteins detected by IB following FLAG IP from 293T cells expressing the indicated plasmids. In (D) samples from time 0 for cell lines shown in Figure 4C were loaded together for comparison. (E) Primary adult skin fibroblasts of the indicated genotypes expressing the indicated plasmids and following treatment with cycloheximide (CHX) for the indicated times. (F) Transcripts measured by qPCR in primary adult skin fibroblasts expressing the indicated shRNA. (G) Primary adult skin fibroblasts from *Fbxw7*^{FL/FL} mouse +/- CRE recombinase (Ad-CRE) expressing the indicated plasmids and following treatment with cycloheximide (CHX) for the indicated times. In (H) samples from time 0 for cell lines shown in Figure S4G were loaded together for comparison. (I) Transcripts measured by qPCR in primary adult skin fibroblasts from (G). In (F,H) * $P < 0.05$, ** $P < 0.01$, *** $P < 0.005$

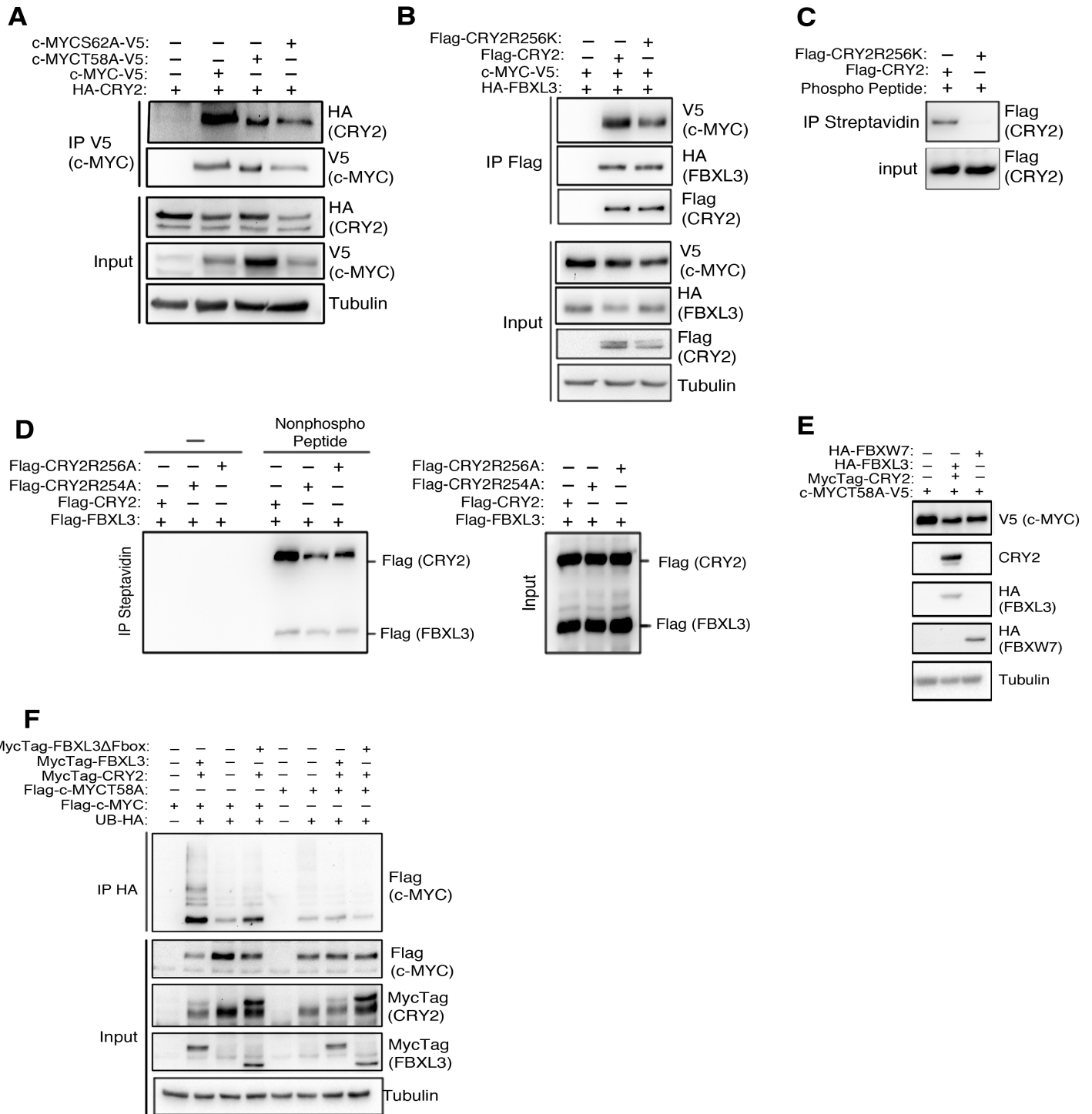


Figure S5. Related to Figure 5. SCF^{FBXL3+CRY2} interacts specifically with T58-phosphorylated c-MYC

Proteins detected by IB following FLAG IP (A,B) or HA IP (F) or in whole cell lysates (E) from 293T cells expressing the indicated plasmids (A,B,E,F) or following streptavidin affinity purification after incubation of purified Flag-CRY2 and/or Flag-FBXL3 with the indicated biotinylated peptides (C,D). In (E) samples from time 0 for cell lines shown in Figure 5F were loaded together for comparison.

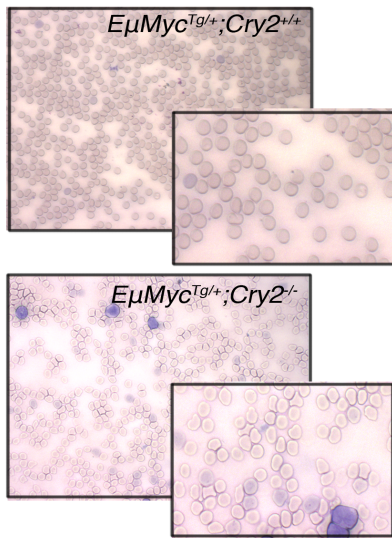
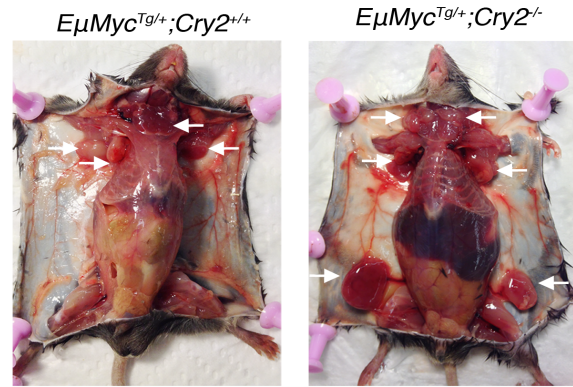
A**B**

Figure S6. Related to Figure 7. CRY2 deletion enhances MYC-driven lymphoma in vivo

(A) Representative Giemsa-stained blood smears prepared from circulating blood of 6-week-old $E\mu\text{Myc}^{+/+};\text{Cry2}^{+/+}$ and $E\mu\text{Myc}^{+/+};\text{Cry2}^{-/-}$ littermates. (B) Typical appearance of lymphomas at time of sacrifice due to advanced disease progression in $E\mu\text{Myc}^{+/+};\text{Cry2}^{+/+}$ and $E\mu\text{Myc}^{+/+};\text{Cry2}^{-/-}$ littermates.

Table S1: Average Read Counts for Differentially Expressed Genes, Related to Figure 2.

Average read counts from deep sequencing of RNA isolated from wildtype and *Cry2*^{-/-} MEFs at four hour intervals after synchronization of circadian rhythms with dexamethasone. All genes determined to be differentially expressed between genotypes are included (FDR < 0.01). WT0, WT4, WT8, WT12, WT16, and WT20 denote readings from RNA isolated from wildtype MEFs collected at 0, 4, 8, 12, 16, and 20 hours after dexamethasone treatment. KO0, KO4, KO8, KO12, KO16, and KO20 denote readings from RNA isolated from *Cry2*^{-/-} MEFs isolated at 0, 4, 8, 12, 16, and 20 hours after dexamethasone treatment.

Table S2: Average Read Counts for Hallmark pathway MYC targets V1, Related to Figure 2.

Average read counts from deep sequencing of RNA isolated from wildtype and *Cry2*^{-/-} MEFs at four hour intervals after synchronization of circadian rhythms with dexamethasone for genes included in the Hallmark gene set of c-MYC targets. WT0, WT4, WT8, WT12, WT16, and WT20 denote readings from RNA isolated from wildtype MEFs collected at 0, 4, 8, 12, 16, and 20 hours after dexamethasone treatment. KO0, KO4, KO8, KO12, KO16, and KO20 denote readings from RNA isolated from *Cry2*^{-/-} MEFs isolated at 0, 4, 8, 12, 16, and 20 hours after dexamethasone treatment.

Table S3. Human cancer cell (CCLE) lines ranked by *CRY2* copy number, *CRY2* expression, and tumor type, Related to Figure 6.

CRY2 genomic copy number ('CopyNumber') and RNA expression ('ExpressionMASS') extracted from microarray data (probeset 212695_at) for human cancer cell lines in the Cancer Cell Line Encyclopedia (CCLE). Descriptions include the cell line names, lineage, cancer subtype, primary site, and histological classification as well as the *CRY2* copy number and RNA expression data.

EXTENDED EXPERIMENTAL PROCEDURES

Plasmids pcDNA3-2xFlag-mCRY1, pcDNA3-2xFlag-mCRY2 are as described previously (Lamia et al., 2009). mCRY2, FBXL3 and Human c-MYC coding sequences were transferred to pcDNA3.1-based HA-epitope, pcDNA3.1-based Flag-epitope or pBABE puro-based vectors using standard protocols. cDNA encoding full length human c-MYC were generated by RT-PCR from RNA extracted from 293T cells. Plasmids expressing c-MYC protein were made by cloning the cDNA into a pcDNA3.1-based V5-epitope tagged vector using the pcDNA Gateway Directional TOPO Expression Kit (Invitrogen #K2440-20). All mutations were introduced using Agilent Site-Directed Mutagenesis kit and protocols (cat # 200521). pWZL Blast MYC deposited by Dr. William Hahn was purchased from Addgene (Addgene plasmid 10674) (Boehm et al., 2005). psPAX plasmid (Addgene plasmid 12260) and pMD2.G plasmid (Addgene plasmid 12259) deposited by Dr. Didier Trono, and used for infection, were also purchased from Addgene. pBABE-Puro, pWZL hygro, pWZL hygro HRAS^{V12} and pMLH-shRNA p53 were gifts from Dr. Tyler Jacks (MI, Boston, MA). The following shRNAs were purchased from Sigma and their efficacy was confirmed: pLKO.1 shRNA Fbxl3#1 (TRCN0000126944); shRNA Fbxl3#2 (TRCN0000126946); shRNA Fbxl3#3 (TRCN0000369031); shRNA Fbxl3#4 (TRCN0000369032), shRNA Fbxw7#1 (TRCN0000006555); shRNA Fbxw7#2 (TRCN0000235421). pLKO.1 sh_scramble deposited by Dr. David Sabatini

was purchased from Addgene (Addgene plasmid 1864) (Sarbassov et al., 2005). Ub-HA was a gift from Dr. Tony Hunter. pLV-CMV-CRE and pLV-CMV-GFP plasmids were a gift from Dr. Anastasia Kralli and are available through Addgene.

Cell Culture and Transfection HEK293T (293T), A549, and SW480 cells were purchased from the American Type Culture Collection (ATCC). Three different series of MEF cells were isolated from embryos of the indicated genotypes at E15.5. Two different series of adult skin fibroblasts were prepared from ear biopsies of adult mice of the indicated genotypes, as described previously (Papp et al., 2015) or from $Fbxw7^{lox/lox}$ adult mice (B6;129Fbxw7^{tm1laai}/J; Jackson Labs stock #0175663). All MEFs and adult skin fibroblasts (ASFs) were used as primary (passaged no more than 10 times and grown in 3% oxygen) or spontaneously immortalized. MEF and 293T cells were grown in complete Dulbecco's Modified Eagle Medium (DMEM) (Invitrogen cat #10569), A549 and SW480 were grown in RPMI 1640 (Invitrogen cat #10491). 293T, A549 and SW480 cell media were supplemented with 10% fetal bovine serum, and 1% penicillin and streptomycin. MEF and ASF media were supplemented with 15% fetal bovine serum, and 1% penicillin and streptomycin. 293T, A549, and SW480 cells were grown in a 37°C incubator maintained at 5% CO₂ and 20% O₂ (high oxygen). MEFs and ASFs were grown in a 37°C incubator maintained at 5% CO₂ and 3% O₂ (low oxygen). Transfections were carried out using polyethylenimine (PEI; Polysciences Inc cat #23966-2) or calcium phosphate following manufacturer instructions using 1 to 5 µg of DNA. Cycloheximide (CHX) (Fisher cat # 50255724) was used at a concentration of 100 µg/ml as indicated. Dexamethasone 21-phosphate sodium salt (Sigma cat #D1159) was used at a concentration of 1 nM. For the ubiquitylation assay, cells were pre-treated for 4 or 6 hours with MG132 (Calbiochem cat # 474790) at a concentration of 10 µM.

Generation of Viruses and Stable Cell Lines Lentiviral shRNA were produced by transient transfection into HEK 293T cells using psPAX and pMD2.G packaging plasmids for virus generation. Lentiviral supernatants were harvested 48 hours after transfection, filtered through a 0.45 µm filter, supplemented with 6 µg/ml polybrene (Sigma) and added to parental cell lines. After 6 hours, additional medium was added to dilute the polybrene to < 3 µg/ml. 48 hours after viral transduction, the infected cells were split into selection media containing 2 µg/ml of puromycin (Sigma), 5 µg/ml of blasticidin (Invitrogen) or 75 µg/ml of hygromycin (Sigma). Selection media were replaced every 2-3 days until selection was complete (2 days to 2 weeks).

Proliferation and Transformation Assays For proliferation analysis, cells were seeded in 6-well plates at 5,000 cells/well. Cells were counted using a Moxi Z cell counter and S cassettes (VWR) every 2 days for 6 to 10 days. For the colony formation assay, 1,000 cells were plated in 10cm plates and grown for 2 to 3 weeks prior to staining with 0.005% Crystal violet. Three independent experiments were carried out for each assay. For the anchorage independent growth, cells were suspended in complete medium containing 0.4% low melting agarose and plated in 6-well plates at a density of 20,000 cells per well, onto solidified 0.8% agarose containing DMEM or RPMI 1640 for MEFs or SW480 and A549 respectively. Cells were grown for 2 to 3 weeks at 37°C prior to staining with 1mg/ml MTT (Life Technologies #M-6494) for 1 hour.

Immunoprecipitation and Western Blotting 293T whole cell extracts were prepared using lysis buffer containing 1% TX-100 as previously described (Lamia et al., 2004). MEF cell extracts were prepared from RIPA

buffer containing 1% TX-100, 147mM NaCl, 12mM sodium deoxycholate, 0.1% SDS, 50mM Tris pH 8.0, 10mM EDTA, 50 μ M PMSF, 1mM β -Glycerophosphate, 1mM Sodium Orthovanadate and protease inhibitors (Roche catalog # 11697498001). Antibodies used for immunoprecipitation were anti-Flag M2 agarose beads (Sigma cat # A2220), anti-V5 agarose beads (Sigma cat # A7345), and monoclonal anti-HA agarose beads (Sigma cat # A2095). Antibodies for Western blot were anti-Flag polyclonal (Sigma cat # F7425), anti-V5 polyclonal (Bethyl cat # A190-120A), anti-HA polyclonal (Sigma cat # H6908), anti-LaminA (Sigma cat # L1293), anti- β -Tubulin (Sigma cat # T5168), anti- β -Actin (Sigma cat # A1978), CRY1-CT and CRY2-CT as described (Lamia et al., 2011), anti-c-MYC (Abcam cat # ab32072), and anti-Cullin (Life Technologies cat # 71-8700).

***In vivo* ubiquitylation assay** 293T cells were co-transfected with Flag-MYC, Flag-MYC T58A, Myc-FBXL3, Myc-CRY2 and HA-tagged ubiquitin. Cells were pre-treated for 6 hours with MG132 (Calbiochem cat # 474790) at a concentration of 10 μ M and cell extracts were prepared using lysis buffer containing 1% TX-100 as previously described (Lamia et al., 2004) supplemented with 1mg/ml of iodoacetamide. We used monoclonal anti-HA agarose beads to purify ubiquitinated proteins. Precipitates were analyzed by immunoblot with anti-c-MYC (Abcam cat # ab32072) or an anti-Flag polyclonal (Sigma cat # F7425)

Nuclear and Cytoplasmic Fractionation of Cultured Cells Cells were washed once with ice cold PBS, fresh cold PBS was added and the cells were transferred to a 5 ml tube and centrifuged 5 minutes at 2000 rpm. The resulting pellets were washed with cold PBS and transferred to 1.5-ml eppendorf tubes and centrifuged 5 minutes at 2000rpm. The resulting pellets were resuspended in Solution A (10 mM Hepes pH 8, 1.5 mM MgCl₂, 10 mM KCl, plus protease and phosphatase inhibitors), and incubated for 15 minutes at 4°C. An equal volume of Solution B (Solution A + 1% NP40) was added and the samples were further incubated for 5 minutes at 4°C, and centrifuged 5 minutes at 3000 rpm. Supernatants from this step represent the cytoplasmic fraction. The remaining nuclear pellets were then washed twice with cold PBS, lysed in RIPA buffer, and either used directly (nuclear lysates) or diluted 6-fold into IP buffer for immunoprecipitation.

Peptide Binding Assay Whole cell extracts were prepared from 293T cells previously transfected using PEI with the indicated Flag-tagged constructs (2 plates per condition for Flag-FBXL3 and 1 plate per condition for Flag-CRY2 or Flag-CRY2 mutants) using lysis buffer containing 1% TX-100 as previously described (Lamia et al., 2004). The whole cell extracts from all Flag-Fbxl3 transfected plates were then combined, as were the extracts from all Flag-CRY2 transfected plates. The combined whole cell lysates were incubated with anti-Flag M2 agarose beads (Sigma cat # A2220) overnight at 4°C while nutating. The next morning the beads were washed 4X with a RIPA-like buffer containing 50mM Tris pH 7.5, 150mM NaCl, 5mM EDTA, 2mM DTT, 0.5% sodium deoxycholate, 0.05 mM PMSF, 1mM NaF, 1mM sodium orthovanadate, 1mM β -Glycerophosphate, 1% TX-100, and protease inhibitor (Roche cat #11697498001). After washing, the anti-Flag M2 beads were incubated with 3X Flag peptide (Sigma cat# F4799), diluted 1:50 in TBS, for 1.5 hours at 4°C while nutating. The elution was collected and 1/20 of the elution was run on an 8% SDS-PAGE gel. The gel was stained with Coomassie blue and the proteins were quantified relative to a standard curve of BSA run on the gel along with the samples. After quantification, the same amounts of Flag-FBXL3 and Flag-CRY2 were then aliquoted into the following conditions: Flag-CRY2; Flag-FBXL3; Flag-CRY2 and Flag-FBXL3 combined; or each Flag-CRY2 mutant and Flag-

FBXL3 combined. Note that proteins should always be freshly made; phospho-specific binding is lost after storage. Biotinylated synthetic peptides were then added to each condition as shown at a concentration of 10ug per condition. The peptides and eluted protein were incubated together at 30°C for 30 minutes while shaking. After incubation, 1 mL of Streptavidin buffer containing 5mM PBS 7.2, 0.1% SDS, 1% NP-40, 1mM NaF, 1mM sodium orthovanadate, and 1mM β -Glycerophosphate was added to each condition along with 10 μ L of Streptavidin beads (Fisher Scientific cat # PI20349) and incubated overnight at 4°C while nutating. The next morning the beads were washed 3X with the same Streptavidin buffer additionally containing 0.5% sodium deoxycholate, and then samples boiled with protein sample buffer. The custom synthetic peptides used in this assay (NP: Biotin-Ahx-WKKFELLPTPLSPSRRS-amide, P: Biotin-Ahx-WKKFELLP[pT]PPLSPSRRS-amide, DP: Biotin-Ahx-WKKFELLP[pT]PPL[pS]PSRRS-amide) were purchased from 21st Century Biochemicals, Inc. (Marlboro, MA).

Sequential IP Whole cell extracts were prepared from 293T cells previously transfected using PEI with the indicated V5, HA, or Flag-tagged constructs using lysis buffer containing 1% TX-100 as previously described (Lamia et al., 2004). The whole cell extracts were then incubated with anti-Flag M2 agarose beads (Sigma cat # A2220) overnight at 4°C while nutating. The next morning the beads were washed 3X with the same lysis buffer, and incubated in 150 μ L 3X Flag peptide (Sigma cat# F4799), diluted 1:50 in TBS, for 1.5 hours at 4°C while nutating. The eluted peptide was collected from the beads and subsequently incubated with Monoclonal anti-HA agarose antibody beads (Sigma cat # A2095) for 2 hours at 4°C while nutating. The anti-HA beads were then spun down and washed 3X with lysis buffer and boiled with protein sample buffer.

Quantitative RT-PCR RNA was extracted from MEFs with Qiazol reagent using standard protocols (Qiagen cat # 799306). cDNA was prepared using QScript cDNA Supermix (VWR cat # 101414-106) and analyzed for gene expression using quantitative real-time PCR with iQ SYBR Green Supermix (Biorad cat # 1708885). Primers used for qPCR were:

	Forward (5'-3')	Reverse (5'-3')
<i>m-bTrCP2</i>	TGGCGCTATGATGGGAA	GTCAAGAGCAGCCTGCAAGTC
<i>m-Cry1</i>	GCTATGCTCCTGGAGAGAACGT	TGTCCCCGTGAGCATAGTGTA
<i>m-Fbxw7</i>	GAGACTTCATCTCCTTGCTTCTAAA	CGCTTGACAGCAGGTCTTTG
<i>m-Fbxw8</i>	GCCAGGTTGCCTTTGGAGT	TCCCGGATGTTGACACAGGTA
<i>m-Myc</i>	GCGACTCTGAAGAAGAGCAAG	GCCTCGGGATGGAGATGAG
<i>m-Reverb-α</i>	TGAACGCAGGAGGTGTGATTG	GAGGACTGGAAGCTATTCTCAGA
<i>m-Usp28</i>	GGGTCCGAGAAGGAAAGCC	CACGGAACGATCCGAAGGAAG
<i>m-Fbxl3</i>	ACCAC CTACA GTATG TCAGC	AGTCG AGATA AGTCC GAGAG
<i>m-Arntl</i>	TCAAGACGACATAGGACACCT	GGACATTGGCTAAAACAACAGTG
<i>m-Per1</i>	CCCCTGCCTCCCAGTGA	CTGAAAGTGCATCCTGATTGGA
<i>m-Bcl2l11</i>	CCCGGAGATACGGATTGCAC	GCCTCGCGGTAATCATTTC
<i>m-Slc7a5</i>	ATATCACGCTGCTCAACGGTG	CTCCAGCATGTAGGCGTAGTC
<i>m-Ptkb2</i>	TGAGCCCTTGAGCCGTGTA	AGCTTGAAGTTCTCCCTGGG
<i>m-St6gal1</i>	CTCCTGTTTGCCATCATCTGC	GGGTCTTGTGGCTGTTTGAGA
<i>m-Hprt</i>	TGCTCGAGATGTCATGAAGG	TATGTCCCCGTTGACTGAT

Isotope labeling Following dexamethasone-induced synchronization, cells were cultured in glucose free DMEM

(Sigma) containing 15% FBS and 25 mM [$U\text{-}^{13}\text{C}_6$] glucose (Cambridge Isotope Labs) for 10 hours. Polar metabolites and total fatty acids were extracted, derivatized, and analyzed as previously described (Vacanti et al., 2014). To determine ribose enrichment, RNA was isolated from the interface of the MeOH:H₂O:CHCl₃ extraction using TRIzol. Isolated RNA was hydrolyzed via incubation in 2N HCL at 100°C for 2 hours and then dried under airflow at 60°C for 20 minutes. The dried hydrolysate was derivatized via incubation in 30 μ l 2% hydroxylamine hydrochloride in pyridine at 90°C for 60 minutes. 50 μ l propionic anhydride was added and the mixture was incubated at 60°C for 30 minutes before drying under airflow. Derivatized analytes were re-dissolved in 50 μ l ethyl acetate and analyzed via GC-MS using a DB-35MS column (30m x 0.25mm i.d. x 0.25 μ m, Agilent J&W Scientific) installed in an Agilent 7890A gas chromatograph (GC) coupled to an Agilent 5975C mass spectrometer (MS) operating under electron impact ionization at 70 eV. One microliter of sample was injected in splitless mode at 270 °C using helium as the carrier gas at a flow rate of 1 ml/min. The GC oven temperature was held at 100 °C for 1 minute and increased to 280 °C at 20°C per minute. The detector was run in scanning mode, recording ion abundance in the range of 100–605m/z. Ribose mass isotopomer distribution was determined by integrating mass fragments 259 (sum formula: C₁₂H₁₉O₆) and 284 (sum formula: C₁₃H₁₈O₆N) and correcting for isotope natural abundance as described (Fernandez et al., 1996). To determine the percent of newly synthesized palmitate in biomass after tracer addition and the relative contribution of glucose to lipogenic AcCoA, isotopomer spectral analysis (ISA) was employed (Metallo et al., 2012).

RNA Sequencing The 100bp reads are generated by the HiSeq Analyzer 2000 located at the Scripps DNA Sequencing Facility. The Genome Analyzer Pipeline Software (currently Casava v1.8.2) is used to perform the early data analysis of a sequencing run, which does the image analysis, base calling, and demultiplexing. For mRNA-Seq TopHat v2.0.13 with Bowtie2 is currently being used to align to mm10 genome and very sensitive alignment and other default parameters. For the mRNA annotation, Partek[®] software, version 6.6 Copyright © 2012 Partek Inc., St. Louis, MO, USA is used.

Gene Set Enrichment Analysis Gene Set Enrichment Analysis (GSEA) is a computational method that determines whether an *a priori* defined set of genes shows statistically significant, concordant differences between two biological states (e.g. phenotypes). The original paper reporting the method (Subramanian et al., 2007) fully describes the algorithm. Expression levels (RPKM) of all transcripts measured by RNA sequencing in triplicate samples of wildtype (WT) and *Cry2*^{-/-} cells were used as input for Gene Set Enrichment Analysis comparing the two genotypes (WT vs. *Cry2*^{-/-} regardless of circadian time) using the Hallmarks gene set database (Liberzon et al., 2015) in molecular signatures database (MSigDB v5.1).

Structure Modeling Molecular graphics and analyses were performed with the UCSF Chimera package (Pettersen et al., 2004). Chimera is developed by the Resource for Biocomputing, Visualization, and Informatics at the University of California, San Francisco (supported by NIGMS P41-GM103311).

Cell-free Protein Expression Flag-CRY2, FBXL3-V5 and c-MYC proteins were expressed in a cell-free expression system, using the *in vitro* coupled transcription–translation kit TNT T7 Quick for PCR DNA (Promega) according to the manufacturer’s guidelines. The same amounts of newly synthesized Flag-CRY2, FBXL3-V5 and c-MYC

were aliquoted into the following conditions: Flag-CRY2 and FBXL3-V5; Flag-CRY2 and c-MYC ; Flag-CRY2,FBXL3-V5, and c-MYC combined. The proteins were incubated together at 30°C for 1 hour while shaking. After incubation, 1ml of IP buffer containing 0.01% BSA was added to each condition along with 10µL of anti-Flag M2 agarose beads (Sigma cat # A2220), and then incubated for 1h at 4°C while nutating. The beads were washed 4X with a RIPA-like buffer containing 50mM Tris pH 7.5, 150mM NaCl, 5mM EDTA, 2mM DTT, 0.75% sodium deoxycholate, 0.05mM PMSF, 1mM NaF, 1mM sodium orthovanadate, 1mM β-Glycerophosphate, 1% TX-100, and protease inhibitors (Roche cat #11697498001) and then samples boiled with protein sample buffer. The samples were separated by SDS-PAGE and proteins were detected by autoradiography.

Pulse-Chase Labeling Experiment 293T cells transfected with Flag-c-MYC or Flag-c-MYC, HA-CRY2, and FBXL3-V5 combined, were incubated in a Pulse medium (Methionine/Cysteine-free cell culture medium; 10% dialyzed FBS and 1% penicillin and streptomycin) for 30 minutes at 37°C. Proteins were then pulse-labeled with Pulse medium containing ³⁵S-Methionine (³⁵S-Met, 0.1mCi/ml, Perkin Elmer) for 30 minutes at 37°C. The labeling was stopped by replacing the Pulse medium with regular 293T cell culture medium. Cells were collected at the indicated time points. Whole cell extracts were prepared using lysis buffer containing 1% TX-100 as previously described (Lamia et al., 2004) and were incubated with anti-Flag M2 agarose beads (Sigma cat # A2220) overnight at 4°C while nutating. The next morning the beads were washed 4X with a RIPA-like buffer containing 50mM Tris pH 7.5, 150mM NaCl, 5mM EDTA, 2mM DTT, 0.5% sodium deoxycholate, 0.05mM PMSF, 1mM NaF, 1mM sodium orthovanadate, 1mM β-Glycerophosphate, 1% TX-100, and protease inhibitors (Roche cat #11697498001). After washing, the samples were separated by SDS-PAGE and proteins were detected by autoradiography using a Typhoon Trio Imager (GE Healthcare).

Translation Experiment Proteins from adult skin fibroblasts were labeled with Pulse medium containing ³⁵S-Methionine (³⁵S-Met, 0.1mCi/ml, Perkin Elmer) for the indicated times. Whole cell extracts were prepared using lysis buffer containing 1% TX-100 as previously described (Lamia et al., 2004) and were incubated with protein A sepharose (GE Healthcare #17-0886-01) pre-coupled with an anti-c-MYC antibody (Abcam cat # ab32072) overnight at 4°C while nutating. The next morning, cells were washed 4X with the RIPA-like buffer described above except with only 0.5% sodium deoxycholate. The samples were separated by SDS-PAGE. Proteins were detected by autoradiography using a Typhoon Trio Imager (GE Healthcare).

Tissue Expression Profile To investigate the expression profile of *Cry2* in human normal and cancer samples, publicly available microarray data were compiled, normalized and re-analyzed by Novartis bioinformatics group. All microarray datasets were processed using the MAS5 algorithm, with a 2% trimmed-mean normalization to 150. Original data were extracted from GEO database, CCLE database and TCGA database.

Generation of *EμMyc^{+/-}*; *Cry2^{-/-}* mice *Cry2^{-/-}* mice were shared by Dr. Aziz Sancar (Thresher et al., 1998); *EμMyc^{+/-}* mice (Adams et al., 1985) were purchased from Jackson laboratories. *Cry2^{+/-}* females were mated to *EμMyc^{+/-}* males to generate *EμMyc^{+/-}*; *Cry2^{+/-}* mice. *EμMyc^{+/-}*; *Cry2^{+/-}* males were mated to *Cry2^{+/-}* females to generate *EμMyc^{+/-}*; *Cry2^{+/+}* and *EμMyc^{+/-}*; *Cry2^{-/-}* mice used for analysis. The transgene was always inherited through the male. All animals were genotyped twice, once before weaning and when sacrificed. Mice were carefully monitored for systemic signs of illness, including ruffled coats, hunched posture, breathing problems, weight loss or palpable lymphomas. Mice showing any of those signs were sacrificed and autopsied. Tumors

and spleens were harvested and processed as described below. All animal care and treatments were in accordance with The Scripps Research Institute guidelines for the care and use of animals.

Nuclear Extract from Tissue Nuclear extracts from spleen were prepared as previously described (Lavery and Schibler, 1993) by the NUN procedure.

Blood Smear Analysis Before being euthanized, blood from six weeks old littermates, $E\mu Myc^{+/-};Cry2^{+/+}$ and $E\mu Myc^{+/-};Cry2^{-/-}$, was withdrawn from tail vein to prepare blood smears. Slides were stained using May-Grünwald Giemsa (Polysciences Inc. cat # 25038-100, cat # 24981-1, and cat # 24984-1) following the manufacturer's instructions.

Data Analysis and Statistics All experiments were repeated at least three times and results were presented either as one representative experiment or as an average \pm SD. Statistical analyses were done using two-tailed student's t-test or two-way ANOVA. Time-dependent survival in mouse experiments was represented with Kaplan-Meier methods and significance was evaluated with the log-rank test. All statistics were performed using Graph-Pad PRISM (version 6) software.

Supplemental References:

Adams, J.M., Harris, A.W., Pinkert, C.A., Corcoran, L.M., Alexander, W.S., Cory, S., Palmiter, R.D., and Brinster, R.L. (1985). The c-myc oncogene driven by immunoglobulin enhancers induces lymphoid malignancy in transgenic mice. *Nature* 318, 533-538.

Boehm, J.S., Hession, M.T., Bulmer, S.E., and Hahn, W.C. (2005). Transformation of human and murine fibroblasts without viral oncoproteins. *Molecular and cellular biology* 25, 6464-6474.

Fernandez, C.A., Des Rosiers, C., Previs, S.F., David, F., and Brunengraber, H. (1996). Correction of ¹³C mass isotopomer distributions for natural stable isotope abundance. *Journal of mass spectrometry : JMS* 31, 255-262.

Lamia, K.A., Papp, S.J., Yu, R.T., Barish, G.D., Uhlenhaut, N.H., Jonker, J.W., Downes, M., and Evans, R.M. (2011). Cryptochromes mediate rhythmic repression of the glucocorticoid receptor. *Nature* 480, 552-556.

Lamia, K.A., Peroni, O.D., Kim, Y.B., Rameh, L.E., Kahn, B.B., and Cantley, L.C. (2004). Increased insulin sensitivity and reduced adiposity in phosphatidylinositol 5-phosphate 4-kinase beta^{-/-} mice. *Molecular and cellular biology* 24, 5080-5087.

Lamia, K.A., Sachdeva, U.M., DiTacchio, L., Williams, E.C., Alvarez, J.G., Egan, D.F., Vasquez, D.S., Juguilon, H., Panda, S., Shaw, R.J., *et al.* (2009). AMPK regulates the circadian clock by cryptochrome phosphorylation and degradation. *Science* 326, 437-440.

Lavery, D.J., and Schibler, U. (1993). Circadian transcription of the cholesterol 7 alpha hydroxylase gene may involve the liver-enriched bZIP protein DBP. *Genes & development* 7, 1871-1884.

Liberzon, A., Birger, C., Thorvaldsdottir, H., Ghandi, M., Mesirov, J.P., and Tamayo, P. (2015). The Molecular Signatures Database (MSigDB) hallmark gene set collection. *Cell systems* 1, 417-425.

Metallo, C.M., Gameiro, P.A., Bell, E.L., Mattaini, K.R., Yang, J., Hiller, K., Jewell, C.M., Johnson, Z.R., Irvine, D.J., Guarente, L., *et al.* (2012). Reductive glutamine metabolism by IDH1 mediates lipogenesis under hypoxia. *Nature* 481, 380-384.

Papp, S.J., Huber, A.L., Jordan, S.D., Kriebs, A., Nguyen, M., Moresco, J.J., Yates, J.R., and Lamia, K.A. (2015). DNA damage shifts circadian clock time via Hausp-dependent Cry1 stabilization. *eLife* 4.

Pettersen, E.F., Goddard, T.D., Huang, C.C., Couch, G.S., Greenblatt, D.M., Meng, E.C., and Ferrin, T.E. (2004). UCSF Chimera--a visualization system for exploratory research and analysis. *Journal of computational chemistry* 25, 1605-1612.

Sarbassov, D.D., Guertin, D.A., Ali, S.M., and Sabatini, D.M. (2005). Phosphorylation and regulation of Akt/PKB by the rictor-mTOR complex. *Science* 307, 1098-1101.

Subramanian, A., Kuehn, H., Gould, J., Tamayo, P., and Mesirov, J.P. (2007). GSEA-P: a desktop application for Gene Set Enrichment Analysis. *Bioinformatics* 23, 3251-3253.

Thresher, R.J., Vitaterna, M.H., Miyamoto, Y., Kazantsev, A., Hsu, D.S., Petit, C., Selby, C.P., Dawut, L., Smithies, O., Takahashi, J.S., *et al.* (1998). Role of mouse cryptochrome blue-light photoreceptor in circadian photoresponses. *Science* 282, 1490-1494.

Vacanti, N.M., Divakaruni, A.S., Green, C.R., Parker, S.J., Henry, R.R., Ciaraldi, T.P., Murphy, A.N., and Metallo, C.M. (2014). Regulation of substrate utilization by the mitochondrial pyruvate carrier. *Molecular cell* 56, 425-435.